Heat capacity of multilayers of ^{3}He adsorbed on graphite at low millikelvin temperatures

Dennis S. Greywall
AT&T Bell Laboratories, Murray Hill, New Jersey 07974
(Received 14 September 1989)

Precise heat-capacity results are presented for ^{3}He adsorbed on graphite. The temperature range of the data is from 2 to 200 mK, while the coverages span from somewhat below monolayer completion up through five atomic layers. Promotion of atoms into the second, third, and fourth layers is clearly observed. Nuclear-spin exchange energies of the order of a few tenths of a mK are found for the submonolayer incommensurate solid phase. These values differ significantly from those recently inferred from NMR experiments. Data for the second-layer fluid yield ^{3}He quasiparticle effective masses that agree well with the corresponding first-layer values and range from one to five times the bare ^{3}He mass. Prior to third-layer promotion, the second layer undergoes a first-order phase transition. By comparison with the phase diagram for the first layer, the new phase in the second layer is assumed to be a registered solid. Registry is now with respect to the first ^{3}He layer, which continues to exist as a triangular-lattice solid incommensurate with the graphite substrate. The registered phase exhibits a large, sharp heat-capacity anomaly at 2.5 mK. This anomaly may be due to antiferromagnetic polarons which form around zero-point vacancies or may be the signature of an unusual registered phase in which some of the atoms are positioned at substrate potential maxima. As the coverage is increased further, the second-layer spin peak remains located at 2.5 mK but suddenly grows in amplitude, while the temperature dependence above the peak changes from $T^{-0.5}$ towards T^{-2}. The anomaly reaches its greatest magnitude at 0.24 atoms/Å^2 where, perhaps coincidentally, promotion of atoms into the fourth layer also occurs. At this same coverage previous magnetization measurements have shown a large ferromagnetic peak. The heat-capacity data indicate that the ferromagnetic peak occurs when the second layer exists in a state intermediate between a registered solid and the incommensurate solid. Consistent with this observation, the spin system at 0.24 atoms/Å^2 cannot be accurately described by a nearest-neighbor Heisenberg Hamiltonian. This is contrary to the situation at somewhat higher coverages and to the finding from recent magnetization experiments.

I. INTRODUCTION

Heat-capacity measurements[1,2] have traditionally been used to explore the phase diagram of ^{3}He adsorbed on graphite. These measurements have revealed for the case of submonolayer films a fascinating two-dimensional system, which, depending on the density, can exist as a fluid, as a solid registered with respect to the substrate, or as an incommensurate solid. Although studied less extensively,[3,4] the second layer may be even more intriguing, mainly because of the weaker corrugation of the substrate potential experienced by the second-layer atoms.

Somewhat surprising is the fact that none of the heat-capacity measurements has been extended below 50 mK, and it is at these lower temperatures where especially interesting behavior may occur, particularly for the nuclear-spin system. Presumably, the very low-temperature measurements have not been performed previously due to experimental difficulties associated with thermometry and also with thermal equilibrium.

In this paper heat-capacity results are presented for temperatures between 2 and 200 mK and for coverages between roughly one and five atomic layers. This work was motivated by many previous experiments[5–11] involving bulk liquid ^{3}He in contact with various surfaces, which demonstrated unusual magnetic behavior at very low temperatures, and also by recent magnetization measurements[12] for ^{3}He adsorbed on graphite, which showed a large magnetic anomaly at a coverage of a few atomic layers. The new heat-capacity results, as a function of coverage, exhibit many features that correlate closely with special features in the magnetization results. Taken together, the two sets of complementary information suggest an explanation of the magnetic anomaly different from that proposed to explain the magnetization data alone. The anomaly is attributed to the atoms in the second layer, which are now proposed to exist in a state intermediate between a registered phase[13] and a fully incommensurate solid.

Following a review of the experimental details, this paper is broken down into the discussion of various coverage regimes, beginning with the submonolayer incommensurate solid and progressing towards the highest-coverage films where the interpretation of the data becomes more speculative. Throughout, the main focus is on the behavior of the second layer.

II. EXPERIMENTAL DETAILS

A. Calorimeter

A cross-sectional drawing of the cylindrical calorimeter is shown in Fig. 1. The cell is made of high-purity silver and is nearly filled with a bonded stack of Grafoil[14] and silver foil discs. It is rigidly mounted above a flange clamped to a $PrNi_5$ nuclear demagnetization refrigerator with thermally insulating screws and spacers. Thermal connection between the calorimeter and the refrigerator can be made using a superconducting tin heat switch, which is tin soldered to silver rods welded to the cell base and to the support flange. The calorimeter temperature is measured using a cerium-magnesium nitrate (CMN) thermometer of special design[15] externally attached to the base of the cell. Two Pt-W heaters are also mounted on the cell base. Some technical details of the calorimeter are listed in Table I.

The stack consists of 138 layers of 0.13-mm grade GTA Grafoil sheets interleaved with 0.05-mm silver foils and terminated at each end by 1.6-mm thick silver discs. These were sintered into a single mass following the general technique used by Godfrin[16] for Grafoil and copper. Our procedure was to compress the stack by 8% using a simple steel jig and then to bake it at 700 °C for 2.5 h in a flowing ^{4}He atmosphere. When removed from the press, the lamination expanded by roughly 2%. Next the stack was carefully machined to a diameter of 3.4 cm and then encapsulated with 0.08 mm of silver electroplating in order to join all of the silver foils along their perimeters. To allow the ^{3}He sample access to the graphite substrate, 102 1.3-mm-diam holes were drilled through the stack in a close-pack pattern with a center-to-center spacing of 3 mm. In addition, a much larger diameter hole was drilled along the axis of the stack to accept the silver bolt that attached the stack to the base of the cell. After heating and pumping the stack for several days, the surface area was determined using nitrogen adsorption measurements, Sec. II C. The substrate assembly was then sealed into the cell and mounted in the cryostat. With the cell warmed to 50 °C, it was evacuated using a small copper tube (not shown in the figure), which was later crimped closed. The ^{3}He samples entered the cell through a 0.1-mm-i.d. Cu-Ni capillary.

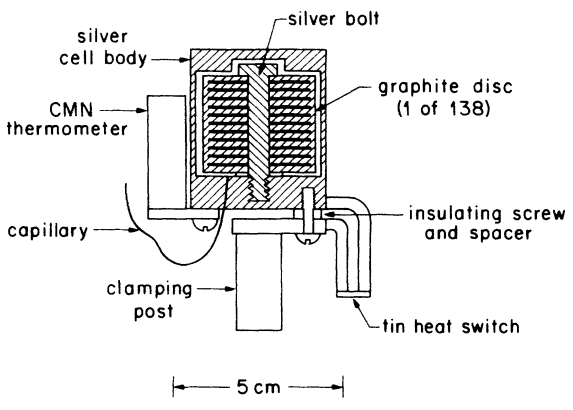

FIG. 1. Calorimeter.

TABLE I. Calorimeter details.

Surface area	203 m^2
Open volume	13.0 cm^3
Heater resistance	436 Ω
Principal construction materials	
Silver	305 g
Copper	15 g
Graphite	14.5 g
CMN	0.1 g

B. Thermometry

The temperature was measured using a CMN thermometer[15] with an extremely fast thermal response. This fast response is a necessity for calorimetry on small thermal mass samples, since even small parasitic heat leaks can cause appreciable temperature drift rates. The response time of a few seconds at 10 mK and of roughly 30 sec at 2 mK is comparable to the thermal equilibrium time of the calorimeter itself.

The responsiveness of the thermometer was achieved by embedding small particles of CMN in a silver matrix. A mixture of CMN and silver powders was compressed into thin pads and simultaneously sintered onto one end of a narrow strip of copper foil. Many of these elements were then epoxied into a single mass and machined to cylindrical shape to accept the coil needed for the self-inductance measurements. A more complete discussion is given in Ref. 15.

The CMN thermometer was calibrated against a ^{3}He melting curve thermometer,[17] mounted on the nuclear cooling stage, for temperatures between 1.8 and 200 mK using the temperature scale of Ref. 11. At higher temperatures the CMN thermometer lacks adequate sensitivity for precise heat-capacity measurements. A more serious problem, however, is the increasing conductance of the tin heat switch. At lower temperatures the range is again limited by the loss of sensitivity, which is now due to the magnetic ordering taking place in the CMN. Another difficulty is the increasing thermal relaxation time.

C. Surface area

The surface area of the graphite substrate was determined using the vapor pressure isotherm of adsorbed nitrogen at 74 K, which is shown in Fig. 2. The short vertical substep in the figure indicates the coexistence[18] of two-dimensional (2D) fluid and solid in registry with the graphite substrate. The high-density end point of the substep corresponds to a completed epitaxial triangular lattice with a particle spacing $\sqrt{3}$ larger than the spacing 2.46 Å, between neighboring graphite hexagons. These numbers imply quite directly that the amount of adsorbed nitrogen measured in cm^3 at standard temperature and pressure (STP) multiplied by 4.223 yields the surface

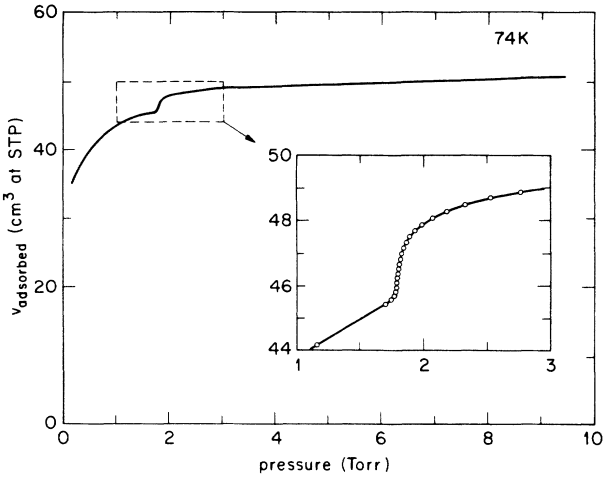

FIG. 2. Vapor pressure isotherm of N_2 on graphite at 74 K. The small substep corresponds to the coexistence of fluid and registered solid and implies a total calorimeter surface area of 203 m^2.

area in m^2. Using 48 cm^3 yields a surface area of 203 m^2, which we expect to be accurate to within a few percent. Indeed, based on this area, the ^{3}He heat-capacity data (Sec. III A) locate second-layer promotion at a coverage of 0.109 atoms/Å^2, and this agrees well with other experimental determinations.[3,19,20]

The specific surface area for the Grafoil in the calorimeter is 14.0 m^2/gm. This value is roughly 20% smaller than the specific area, namely, 17.99±0.17 m^2/gm, determined by Vilches[21] for Grafoil from the same roll but not bonded to metal foils. His value results from a Kr isotherm at 77 K, see Fig. 3. We note that Godfrin[16] found about the same decrease in specific area resulting from his bonding procedure.

D. Procedure

Each measured dosage of ^{3}He was admitted to the calorimeter with the cell regulated at a relatively high temperature in order to produce uniform coverages. The samples with $\rho \leq 0.11$ atoms/Å^2 were held at 4 K overnight. At progressively higher coverages the anneal temperature and time were gradually reduced, corresponding to the increasing sample vapor pressure and were 1.5 K and 2 h, respectively, at our highest coverage of 0.37 atoms/Å.

The ^{3}He-^{4}He mixture that had been pumped from the dilution refrigerator during this process was then recondensed back into the system and cooling was restarted. With a magnetic field of only 4.5 kOe imposed on the $PrNi_5$ nuclear cooling stage, the cryostat reached a temperature of 8 mK in about 16 h. The main heat switch was then opened and the field dropped to zero, causing the calorimeter temperature to decrease to roughly 1 mK in 10 or 15 min.

Next, the current to the heat cell switch solenoid was slowly ramped down to thermally free the calorimeter from the refrigerator. When warming of the cell was first observed, the field reduction was halted leaving the switch partially closed as a compensation for the small parasitic heat leak into the cell. This current was continually adjusted as the cell temperature was increased. Above 50 mK the increasing thermal conductance of the

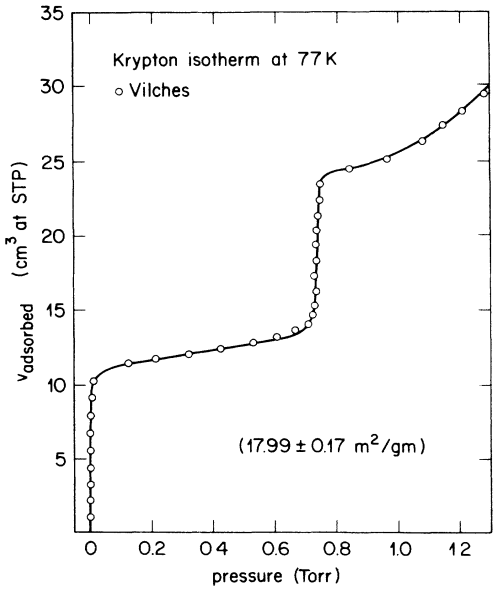

FIG. 3. Vapor pressure isotherm of Kr on graphite at 77 K measured by Vilches. The Grafoil used for these measurements was from the same batch used in this calorimeter but had not undergone any bonding treatment.

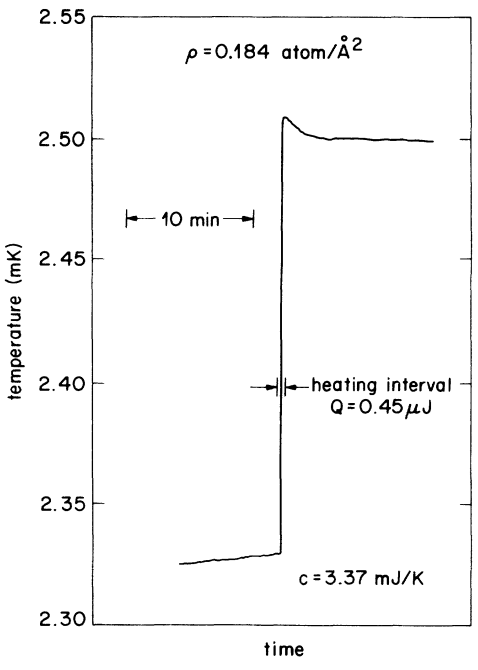

FIG. 4. Typical heat-capacity measurement.

switch in the fully superconducting state became significant. The calorimeter drift rates were then controlled using a second heater mounted on the cell.

The heat capacity was measured using the standard heat pulse technique with heating times in the range 10–40 sec and with temperature steps equal to 5% of the temperature at low temperature and increasing to 30% of T at 200 mK. The larger step sizes were used at the higher temperatures because of the decreasing sensitivity of the CMN thermometer. A typical heat-capacity measurement is shown in Fig. 4. Note the short thermal equilibrium time after the heat pulse.

E. Addendum heat capacity

The addendum heat capacity measured prior to admitting any ^{3}He into the calorimeter is shown in Fig. 5. The large heat capacity at the lowest temperatures is due to

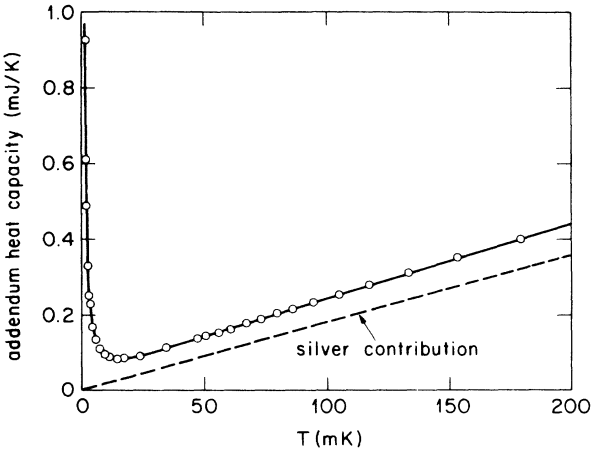

FIG. 5. Addendum heat capacity.

TABLE II. Parameters describing nonspin contributions to the low-temperature heat capacity. β is the amplitude of a nearly-temperature-independent contribution of unknown origin. γ is the coefficient of the term proportional to temperature and associated with a Fermi fluid. Also tabulated are the areal densities of the first, second, and third layers.

n (mol)	ρ (atoms/Å^2)	ρ_1 (atoms/Å^2)	ρ_2 (atoms/Å^2)	ρ_3 (atoms/Å^2)	β (mJ/K)	γ (mJ/K^2)
0.002 662	0.079	0.079	0	0	0	
0.002 831	0.084	0.084	0	0	0	
0.003 373	0.100	0.100	0	0	0	
0.003 704	0.110	0.109	0.001	0		
0.004 043	0.120			0	0.12	23
0.004 381	0.130			0	0.12	29
0.004 715	0.140			0	0.12	40
0.005 055	0.150			0	0.12	55
0.005 397	0.160	0.114	0.046	0	0.12	82
0.005 729	0.170	0.114	0.056	0	0.12	
0.005 899	0.175	0.114	0.061	0	0.12	
0.005 998	0.178	0.114	0.064	0	0.12	
0.006 099	0.181	0.114	0.067	0	0.12	
0.006 200	0.184	0.114	0.0694	0.001	0.123	2.0
0.006 402	0.190	0.114	0.07 276	0.003	0.134	11.6
0.006 740	0.200	0.114	0.07 650	0.010	0.151	19
0.007 077	0.210	0.114	0.07 873	0.017	0.168	26
0.007 413	0.220	0.114	0.08 005	0.026	0.185	33
0.007 752	0.230	0.114	0.08 084	0.035	0.202	42
0.008 087	0.240	0.114	0.08 131	0.045	0.219	50
0.008 424	0.250	0.114	0.08 159		0.236	55
0.008 760	0.260	0.114	0.08 176		0.253	69
0.009 097	0.270	0.114	0.08 185		0.270	93
0.009 434	0.280	0.114	0.08 191		0.287	104
0.009 771	0.290	0.114	0.08 195		0.304	115
0.010 108	0.300	0.114	0.08 197		0.321	124
0.010 445	0.310	0.114	0.08 198		0.338	129
0.010 782	0.320	0.114	0.08 199		0.355	136
0.011 120	0.330	0.114	0.08 199		0.372	157
0.011 456	0.340	0.114	0.08 200		0.389	178
0.011 793	0.350	0.114	0.08 200		0.406	191
0.012 130	0.360	0.114	0.08 200		0.423	203
0.012 470	0.370	0.114	0.08 200		0.440	221

the magnetic ordering of the cerium ions in the CMN thermometer. At higher temperatures the heat capacity is dominated by the electronic contribution from the silver cell body, which is approximated by the dashed straight line in the figure. Presumably the contributions form the Cu-Ni fill capillary and from the impurities in the Grafoil are also making significant contributions to the addendum. Fortunately, none of these gives rise to any large anomalies for temperatures less than 200 mK.

III. RESULTS AND DISCUSSION

A. General comments

The heat capacity of ^{3}He adsorbed on graphite was measured for 33 coverages ranging from less than monolayer completion up through five atomic layers, and for temperatures between 2 and 200 mK. Figure 6 shows the smoothed experimental results for each of these coverages, which are identified by the areal density ρ given in

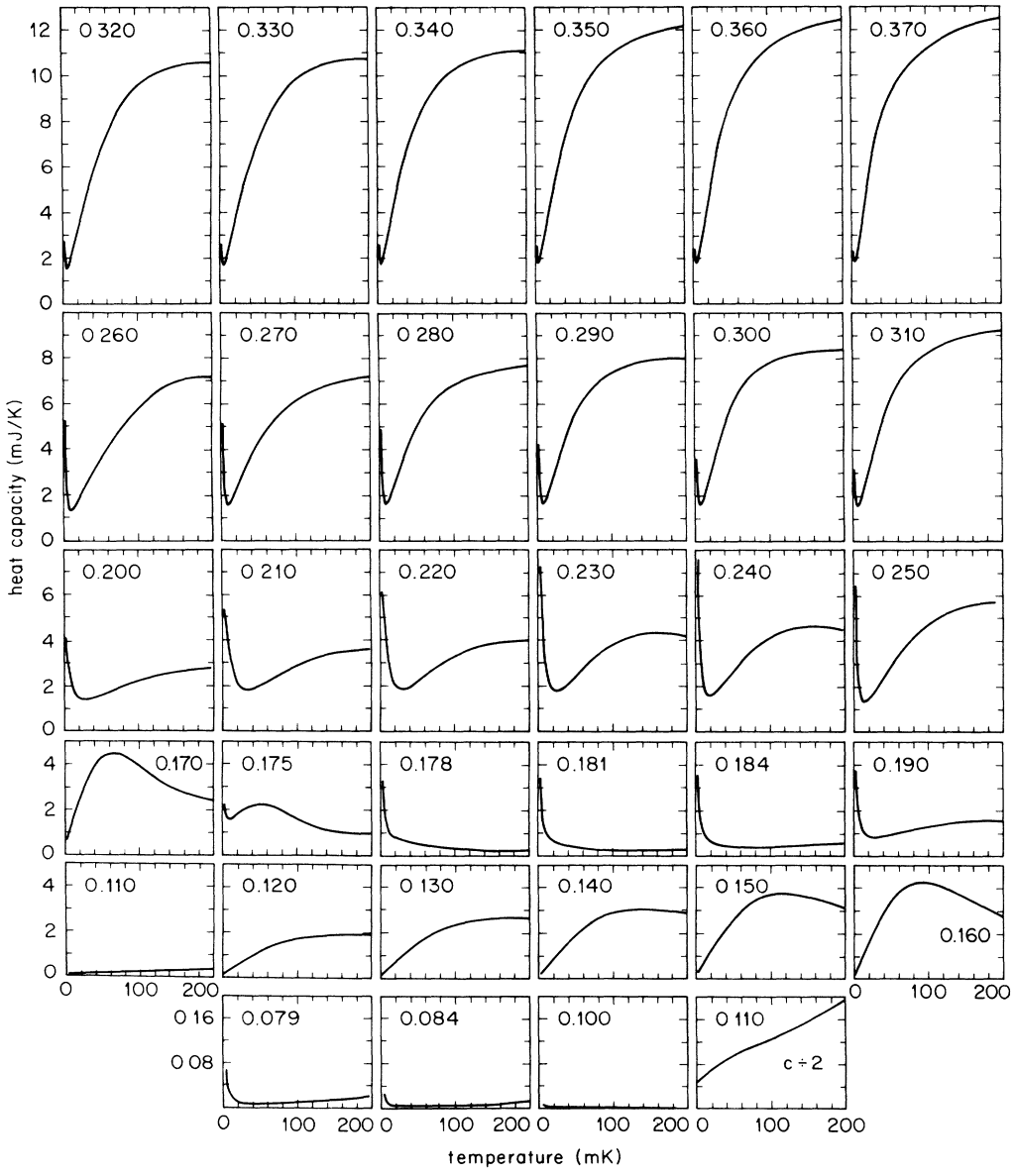

FIG. 6. Smoothed heat-capacity results for each of the samples studied. The numbers give coverages in atoms/Å^2. Note the more sensitive heat-capacity scale for the bottom row of curves.

atoms/Å^2. The approximately 40 data points per curve have not been plotted, since the scatter is only slightly larger than the width of the lines. Other information for each of the coverages is listed in Table II.

The four curves at the lowest coverages are plotted on a heat-capacity scale which is 25 times more sensitive than that for the remainder of the figure. At 0.079, 0.084, and 0.100 atoms/Å^2 the very small heat capacity corresponds to a single layer of two-dimensional solid ^{3}He. The increase in the heat capacity at the lowest temperatures is due to the nuclear-spin contribution. At 0.110 the heat capacity is abruptly much larger, indicating that at this coverage some atoms have been promoted into the second layer. These second-layer atoms comprise a Fermi fluid and dominate the total heat capacity.

The heat capacity then grows continuously as more atoms are added to the second layer. Near 0.170, however, there is a dramatic break away from the lower coverage trend as the second layer solidifies and develops a large nuclear-spin contribution which peaks at 2.5 mK.

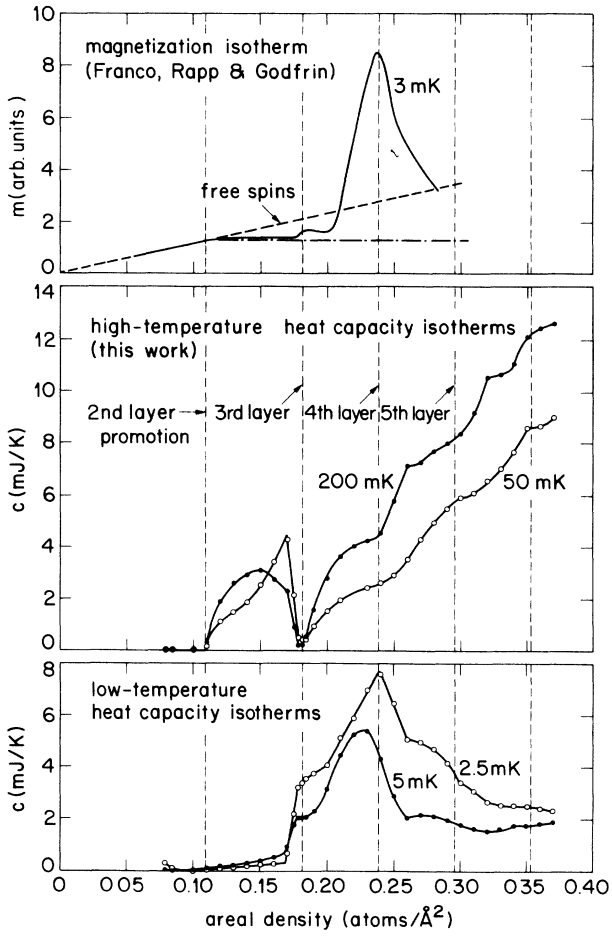

FIG. 7. Heat capacity as a function of coverage for several isotherms. The heat capacity at 2.5 and 5 mK is dominated by the nuclear-spin contribution of the second-layer atoms. The curves at 50 and 200 mK are determined by the fluid contributions from the various layers. Comparison is made with the magnetization results of Franco *et al.*, Ref. 12.

This peak serves as a clear identifier of the second layer. As the coverage is increased still further the heat capacity regains a fluidlike term, showing that atoms are now being promoted into the third layer and eventually into even higher layers.

During this growth of the fluid contribution to the heat capacity, the second layer does not remain as an inert substructure. To the contrary, the second layer undergoes considerable modification as indicated by the behavior of the spin peak which grows to a large maximum at 0.24 atoms/Å^2.

A summary of these heat-capacity results is given in Fig. 7, which shows the heat capacity along several isotherms. The two curves in the bottom portion of the figure show isotherms at 2.5 and 5 mK. At these low temperatures, the nuclear spins provide the main contribution to the heat capacity. The middle portion of the figure displays "high-temperature" isotherms at 50 and 200 mK, where the heat capacity is dominated by the Fermi fluid contributions. These high-temperature isotherms locate second-layer promotion at 0.109, solidification of the second layer between 0.169 and 0.178, third-layer promotion at 0.182, fourth-layer promotion at 0.239, and fifth-layer promotion near 0.296 atoms/Å^2.

The low-temperature isotherms corroborate the coverage location of the second-layer solidification and show the evolution of the nuclear-spin peak. The anomaly reaches its maximum amplitude at a density which also corresponds to fourth-layer promotion.

For comparison, the top part of Fig. 7 shows the 3-mK magnetization isotherm of Franco *et al.*[12] Their curve exhibits a small anomaly, positioned at a coverage where we find second-layer solidification, and a large ferromagnetic peak accurately centered at the same coverage as the heat capacity anomaly. Further discussion of the heat-capacity results is broken down into several coverage ranges and begins with the data obtained for monolayer films.

B. First layer solid; $0.079 \leq \rho < 0.110$ atoms/Å^2

In this coverage regime the ^{3}He atoms are located only in the first layer and comprise a two-dimensional (2D) solid arranged on a triangular lattice. This lattice is incommensurate with the graphite substrate.

For temperatures greater than a few mK, the heat capacity of this ^{3}He layer is dominated by the phonon contribution, which can be described by the 2D Debye relation[2]

$$c_{\text{phonon}} = 28.848 nR (T/\Theta_D)^2 . \quad (1)$$

Heat-capacity measurements[22] that extend up to temperatures of a few degrees yield values of Θ_D that are of the order of 20 K and that increase with areal density roughly as ρ^3.

At very low mK temperatures the heat capacity is almost entirely due to the ordering of the nuclear spins that have an effective interaction due to atomic exchange of less than 1 mK. For temperatures large compared to the exchange energy J, the spin heat capacity is expected to

be given by

$$c_{\text{spin}} = \tfrac{9}{4} nR \left[\frac{J}{k_B T} \right]^2 . \quad (2)$$

The exchange energy in bulk solid ^{3}He is extremely sensitive to the interatomic spacing, a_{NN}; in fact, it is found that $J \alpha a_{\text{NN}}^{50}$. If this same power-law dependence persists for the 2D solid, then $J \alpha \rho^{-25}$.

Consequently, as the areal density increases, both the phonon and spin contributions to the heat capacity should decrease rapidly. The data in Fig. 6 at 0.079, 0.084 and 0.100 atoms/Å^2 show this qualitative behavior.

Figure 8 is a log-log plot of data obtained at 0.0785 atoms/Å^2 in a different cool down of the apparatus. These data have a somewhat higher precision than the 0.079 atoms/Å^2 data of Fig. 6 and clearly show the crossover from the nuclear-spin regime to the lattice phonon regime. A two-term least-squares fit of these data yielded $J/k_B = 0.3$ mK and $\Theta_D = 17$ K. This Debye temperature is 20% smaller than the value measured by Hering and Vilches[22] at this density, but this is easily within our uncertainty. The large uncertainty is due to the sample heat capacity being only a few percent of the addendum contribution near 200 mK.

Near 5 mK the sample heat capacity is 35% of the addendum and so the uncertainty in J is smaller. This uncertainty could be reduced further if it were possible to make reliable measurements at lower temperatures. Unfortunately, the problem then becomes the increasing relaxation time for our thermometer and the fast drift rates associated with the small total heat capacity.

The values of J obtained for the monolayer solid are plotted in Fig. 9 as a function of the nearest-neighbor distance, $a_{\text{NN}} = 1.0746\, \rho^{-1/2}$. Comparison is made with the exchange energies inferred from spin-lattice relaxation measurements at 1.2 K by Cowan *et al.*,[23] open circles, and with the J values for bulk bcc ^{3}He, dashed curve.

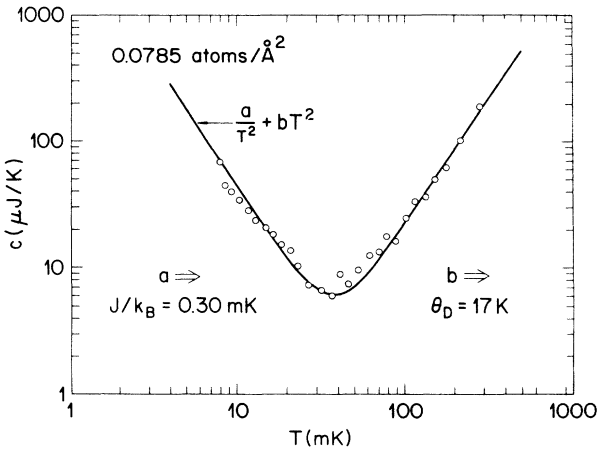

FIG. 8. Log-log plot of the heat capacity of an incommensurate solid ^{3}He monolayer. Below 30 mK the heat capacity is dominated by the nuclear spins and at higher temperatures by the phonons.

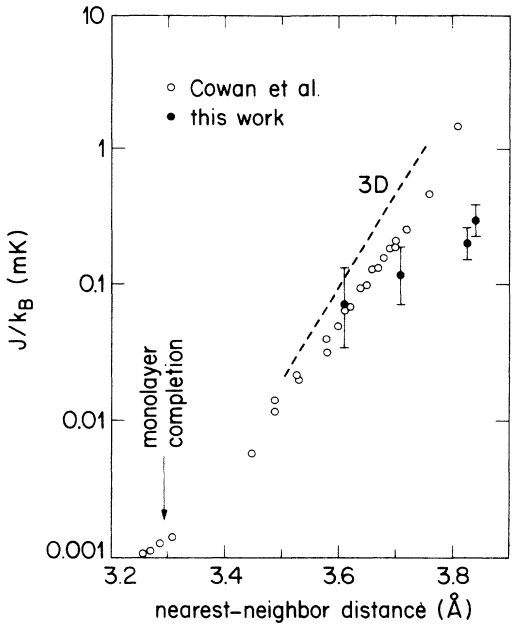

FIG. 9. Exchange energy of the incommensurate solid ^{3}He monolayer. Comparison is made with values inferred from spin-lattice relaxation measurement by Cowan *et al.*, Ref. 23.

The only other estimates of J are from magnetization measurements by Godfrin.[24] He gives an upper limit for J of 50 μK at 3.8 Å. This limit is an order of magnitude smaller than our value, which in turn lies an order of magnitude below the low-density exchange energies from the T_1 measurements. It might be argued that the discrepancy with the J's from the T_1 measurements indicates a problem with the specific model used to extract these latter energies or that thermal vacancies are playing an important role, but there should be little ambiguity in the exchange energies determined by either the heat capacity or the magnetization measurements. An explanation may be that the straightforward comparison of these very different types of experiments is invalid because of the importance of higher-order exchange processes.

C. Second layer fluid; $0.110 \leq \rho \leq 0.160$ atoms/Å^2

This coverage regime begins with ^{3}He atoms being promoted into the second layer, on top of a first layer which exists as a high-density incommensurate solid. The second-layer atoms comprise a two-dimensional (2D) Fermi fluid as identified by a large heat capacity that is linear in temperature below roughly 50 mK.

The heat capacity of an ideal 2D Fermi fluid in the low-temperature limit ($T \ll T_F$) is given by

$$c = \frac{\pi^2}{3} N_2 k_B \frac{T}{T_F} \quad (3)$$

with

$$T_F = \frac{\pi \hbar^2}{k_B m_3} \frac{N_2}{A} . \quad (4)$$

Here A is the total surface area. At high temperatures the heat capacity tends toward $N_2 k_B$. Note that combining Eqs. (1) and (2) to eliminate T_F leads to a cancellation of the number of second-layer atoms N_2 and to the expression.

$$\frac{c}{T} = \frac{\pi k_B^2 m_3}{3\hbar^2} A = 8.986 \times 10^{-2} A \ ; \quad (5)$$

the ideal low-temperature heat capacity in 2D depends only on A and not on N_2. The numerical factor in Eq. (5) is used to determine c/T in mJ/K^2 when A is measured in m^2.

Figure 10 shows the second-layer heat capacity obtained below 40 mK for coverages between 0.11 and 0.17 atoms/Å^2. Actually plotted is the total sample heat capacity, but the contribution from the first layer is extremely small, and no correction was applied. An immediate observation is that none of the curves extrapolates to the origin. However, except for the lowest- and highest-density data, which will be discussed separately, each of the remaining curves has a common $T=0$ intercept β of 0.12 mJ/K.

The source of this excess heat capacity is unknown. It develops as the first atoms are promoted into the second layer and over our temperature range appears to be temperature independent. Assuming a classical specific heat of k_B per "particle," β corresponds to 15 μmol or to one particle for every 2500 Å^2 of surface area. If the homogeneous areas on our graphite substrate have a typical diameter of 100 Å, then we have at most a few particles per homogeneous region. Assuming that these particles have the mass of a ^{3}He atom leads via Eq. (4) to a characteristic temperature of roughly 20 mK, which is much higher than the inferred temperature. This suggests an effective mass that is much larger than m_3.

We note that a qualitatively similar result was observed in measurements of the heat capacity of ^{3}He adsorbed on silver powder.[25] Quantitatively, however, the effect in this latter experiment was 20 times larger. It was also evident that the characteristic temperature was less than 1 mK. Because the excess heat capacity is much smaller on the higher-quality surface provided by the graphite, it may be that this anomaly should be associated in some way with surface inhomogeneities. In the following we simply assume that the excess heat capacity is a constant contribution from an unspecified independent system. The ideal gas curve in Fig. 10 is therefore drawn shifted upward by the constant β, where it appears as a reasonable low-coverage limiting behavior for the data obtained with $\rho \geq 0.12$ atoms/Å^2.

The curve shown for a coverage of 0.11 atoms/Å^2 might appear to be inconsistent with the data obtained at higher coverages, but here the second-layer coverage, and consequently also the Fermi temperature, is extremely small. These data are therefore not in the low-temperature regime, $T \ll T_F$, and cannot be directly compared with the higher-coverage data shown in Fig. 10. A quantitative analysis of the data at 0.11 atoms/Å^2 is also complicated by the fact that the excess heat capacity at this coverage has not yet grown to the limiting value β.

As will be discussed in the following section, the curve at 0.17 atoms/Å^2, which departs from the trend of the lower-coverage data, actually corresponds to two-phase, liquid-solid coexistence. Contrary to what one might have expected, the very-low-temperature heat capacity is larger than the pure liquid term because of a large nuclear spin contribution to the solid heat capacity.

Figure 11 shows the low-temperature, second-layer fluid heat capacity divided by the temperature to exaggerate the deviations from linear behavior and also to demonstrate the density independence of the β parameter. With the same value of β, namely, 0.12 mJ/K, each

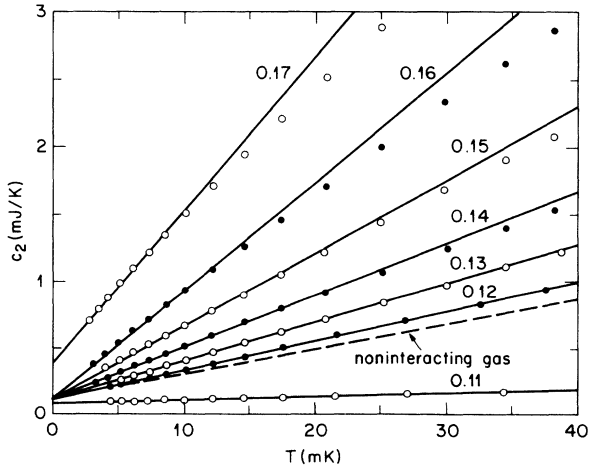

FIG. 10. Low-temperature heat capacity of the second-layer fluid. The numbers give the total coverage in atoms/Å^2.

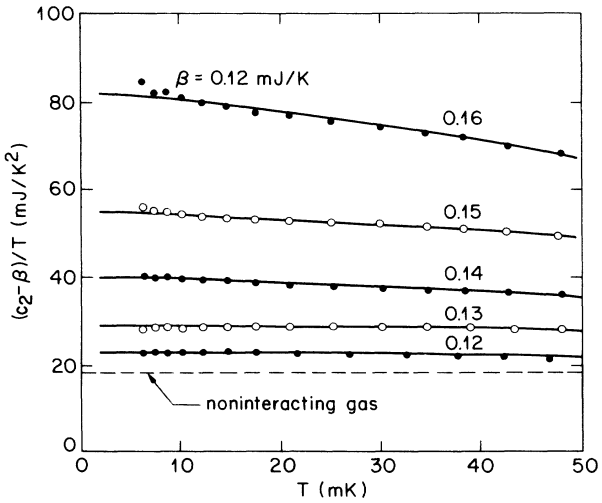

FIG. 11. Second-layer fluid heat capacity divided by the temperature. The parameter β corresponds to an unexplained temperature-independent contribution to the heat capacity that develops as the first atoms are promoted into the second layer. The numbers give the total coverage in atoms/Å^2.

of the curves tends towards temperature independence at low temperature as we would expect for a Fermi fluid. The range over which the heat capacity is accurately proportional to temperature shrinks as the density increases and is less than 10 mK at the highest density. This is very similar to the findings for bulk liquid ^{3}He.[26]

The departures of the lowest-temperature data away from ideal behavior can be attributed to an effective ^{3}He mass, which is larger than the bare mass. The modified form of Eq. (5), can then be rearranged to give

$$\frac{m^*}{m}=\frac{3\hbar^2}{\pi k_B^2 m A}\frac{c_{\text{fluid}}}{T}=\frac{11.13}{A}\frac{c_{\text{fluid}}}{T}\ , \tag{6}$$

where the numerical factor is for c_{fluid}/T in mJ/K^2 and A in m^2. This equation and the vertical-axis intercepts read from Fig. 11 give the values of m^*/m plotted in Fig. 12 as a function of ρ_2. Here it is assumed that $\rho_2=\rho-0.109$ even though ρ_1 is changing by a few percent over this total coverage range. The open circles shown in the figure are the second-layer-fluid effective masses measured by Van Sciver and Vilches,[3] and the open triangles are the first-layer masses measured by McLean.[27] The rather large discrepancy at the higher densities is related at least in part to the earlier measurements extending down in temperature only to 50 mK and therefore not into the fully degenerate regime; see Fig. 11.

The Fermi temperature can be computed using these effective masses and Eq. (4), which can be written

$$T_F=50.54\rho_2 m_3/m_3^*\ . \tag{7}$$

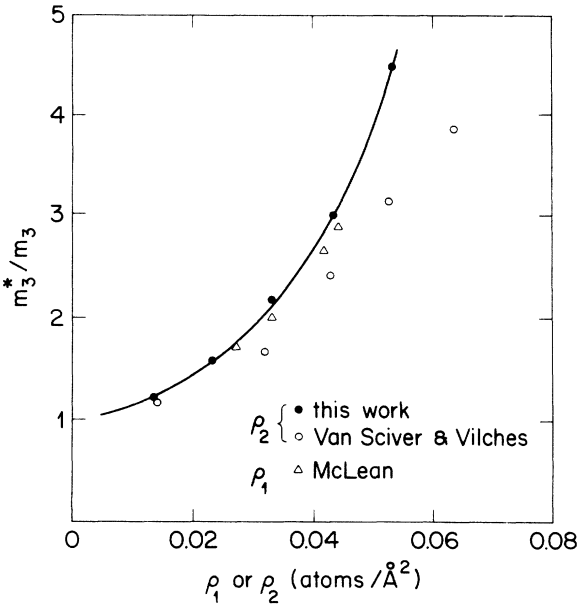

FIG. 12. Effective masses for the first- and second-layer fluids extracted from heat-capacity data. The open circles are from the work of Van Sciver and Vilches; Ref. 3; the triangles are from McLean, Ref. 27.

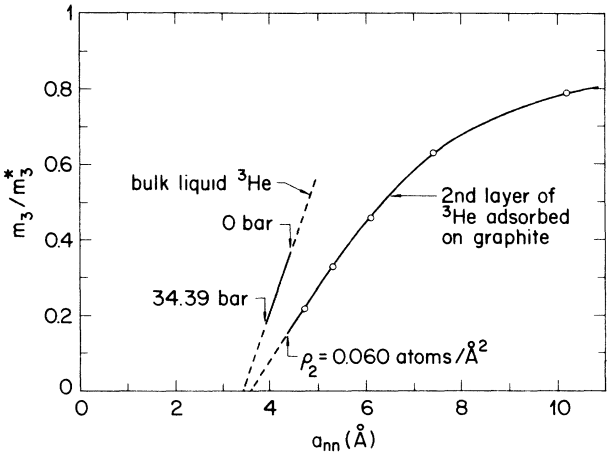

FIG. 13. Comparison of the 2D and 3D fluid effective masses. At the same nearest-neighbor distance the 2D masses are much larger than the 3D values.

At $\rho_2=0.011$, $T_F=0.44$ K; at $\rho_2=0.031$, $T_F=0.72$ K; and at $\rho_2=0.051$, $T_F=0.57$ K.

A comparison of the 2D and 3D ^{3}He effective masses is made in Fig. 13, where m_3/m_3^* is plotted versus the nearest-neighbor distance a_{NN}. In three dimensions, a_{NN} is taken to be that determined by a fcc structure, i.e.,

$$a_{\text{NN}}^{\text{3D}}=(4^{1/3}/2^{1/2})\left[\frac{V}{N_A}\right]^{1/3}=1.328V^{1/3}\ , \tag{8}$$

where V is the molar volume in cm^3 and a_{NN} is in Å. In two dimensions a triangular lattice is assumed and

$$a_{\text{NN}}^{\text{2D}}=2^{1/2}/3^{1/4}\rho_2^{1/2}=1.075/\rho_2^{1/2}\ . \tag{9}$$

Over the complete pressure range and to within the precision of the data[11] the results for bulk ^{3}He can be described by the simple, best-fit expression

$$m_3/m_3^*=0.3706a_{\text{NN}}^{\text{3D}}-1.279\ , \tag{10}$$

which implies a divergence of the mass at 3.46 Å. The 2D results cover a much larger range of particle separations but at the higher densities are consistent with the same functional form and with a divergence at a similar nearest-neighbor spacing. The slope, however, is only half of the 3D value implying much stronger interactions in two dimensions at the same particle separation. It is interesting that the largest effective mass measured in either system is roughly $6m_3$. Presumably for an ideal surface, i.e., with no corrugation of the substrate potential, the 2D fluid would extend to $\rho=0.078$, and at this density m_3^*/m_3 would be near 20.

D. Second-layer registered phase; $0.170\le\rho\le0.184$ atoms/Å^2

In this coverage regime the second layer undergoes a first-order solidification[13] as indicated by Fig. 14, which shows the 2.5- and 200-mK heat-capacity isotherms in the vicinity of third-layer promotion. The rapid decrease in the liquid fraction, over the two-phase region, is clearly indicated by the 200-mK isotherm, since at this tem-

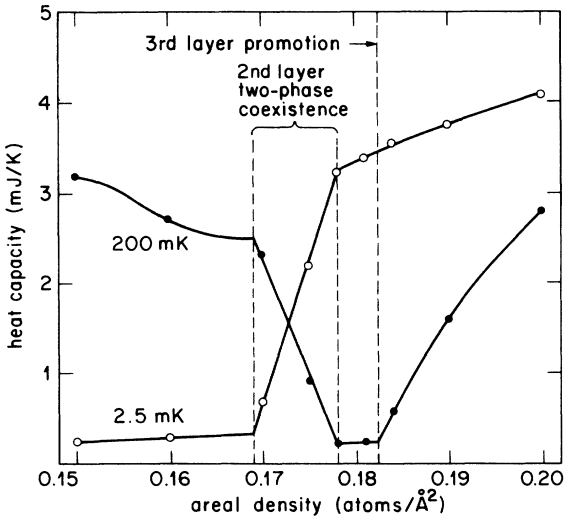

FIG. 14. Heat capacity vs coverage in the vicinity of third-layer promotion. Both the 2.5-mK isotherm (which is dominated by the second-layer nuclear spin contribution to the heat capacity) and the 200-mK isotherm (which is dominated by the second-layer fluid contribution) show a well-defined two-phase coexistence region occurring very near layer promotion.

perature the phonon heat capacity of the solid phase is extremely small. The simultaneous increase in the solid fraction is directly given by the 2.5-mK isotherm as a consequence of the very large nuclear-spin heat capacity at low temperatures. In addition to the obvious two-phase coexistence for $0.169 \leq \rho \leq 0.178$ atoms/Å^2, the linear coverage dependence of both isotherms in this crossover regime confirms the first-order nature of this transition. The abrupt increase at $\rho = 0.182$, which is observed only in the 200-mK isotherm, corresponds to the heat capacity again developing a fluidlike contribution. This is attributed to the promotion of atoms into the third layer. The phase transition in the second layer is therefore complete before a significant number of atoms are promoted into the next level.

Van Sciver and Vilches[3] have also reported a phase transition in the same coverage regime based on heat-capacity measurements at higher temperatures. They concluded that the higher-density phase was a solid that exhibited a melting transition near 1 K. It is interesting that between roughly 0.2 and 0.5 K their solid heat capacity can be described by a term proportional to T^2, as expected for a Debye solid, plus a temperature-independent term. This contribution could be due to a very small number of third-layer atoms, but its magnitude scaled to our cell surface area is 0.12 mJ/K, which is precisely the value of our parameter β determined in Sec. III C using the fluid phase data. This suggests again that the excess heat capacity is due to an independent system and that a simple separation of the various contributions can be made.

Although the heat-capacity measurements indicate a solid second layer near 0.18 atoms/Å^2, neutron scattering experiments[28] performed at 0.203 were interpreted to indicate the absence of a second-layer solid at this coverage. It was this finding, which Franco *et al.*[12] used in support of their model, that located the completion of second-layer solidification at 0.24 atoms/Å^2, corresponding to the peak in their magnetization data; see Fig. 7. An explanation of the neutron results may be that at 0.203 the solid phase does not correspond to a simple triangular lattice. It is also possible that a second-layer solid signal was not observed as a result of experimental difficulties, since a large subtraction had to be made to account for one of the graphite substrate peaks, and the low-density solid may have a large Debye-Waller exponent. More recent neutron scattering experiments[20] at a significantly higher coverage, namely, 0.297 atoms/Å^2, indicate that at this coverage the second layer is indeed solid.

Our belief is that the transition occurring near third-layer promotion is between the fluid phase and a registered solid. This assessment is based primarily on the assumption that the second-layer phase diagram, Sec. III E, is qualitatively similar to that of the first layer and on the very low second-layer density at which the transition occurs. Neutron scattering experiments have shown that when compressed by additional layers the first-layer density is about 5% larger than at second-layer promotion. Our compressed first-layer density should then be 0.114 atoms/Å^2, and the second-layer density should be given by $\rho_2 = \rho - 0.114$. The two-phase region therefore exists for $0.055 \lesssim \rho_2 \lesssim 0.064$, and third-layer promotion occurs at $\rho_2 = 0.068$ atoms/Å^2. At a monolayer coverage of 0.064 the first layer is in $\sqrt{3} \times \sqrt{3}$ registry with the graphite substrate. The monolayer exists as an incommensurate solid only above 0.078.[1,29] A registered second-layer phase is also suggested by the Van Sciver and Vilches results because these authors found that the "melting" peak was detectable only over a narrow range of coverages, as is the case for the registered phase in submonolayer films.

Registry in the vicinity of 0.064 atoms/Å^2 suggests registry again with respect to the graphite substrate. The corrugation in the graphite potential, however, decreases exponentially with distance above the substrate surface[30] and should be negligibly small at the level of the second-layer atoms. It would seem therefore more likely that registry, if indeed it does occur, occurs with respect to the first ^{3}He layer.

The density of the second registered layer relative to the underlying first layer is $0.064/0.114 = 0.56$. The relative coverage for perfect registry, however, might be slightly larger than 0.56 because there may be a range of coverages that should be associated with the registered phase. The phase probably exists with vacancies for $\rho \lesssim \rho_{\text{reg}}$ and with interstitials for $\rho \gtrsim \rho_{\text{reg}}$, but even if an uncertainty of several percent is assigned to this relative density, no simple lattice structure is obviously identified.

Perhaps associated with a more complicated structure is the fact that although more than 95% of the second layer undergoes the transition over a small coverage range, Fig. 14, the remainder transforms at a much slower rate. Figure 15 is a log-log plot of the nuclear-spin contribution to the heat capacity, i.e., the total sam-

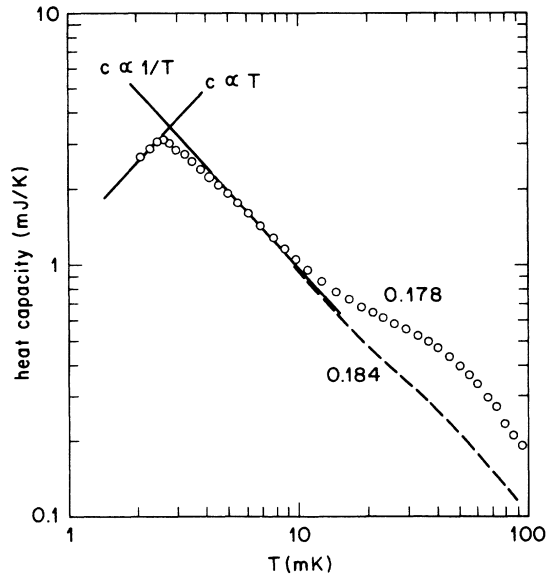

FIG. 15. Nuclear-spin contribution to the heat capacity of the second-layer registered phase. The numbers give the coverages in atoms/Å^2. The rounded bump in the data near 50 mK is presumably a remnant of the fluid phase and may be a consequence of the finite-sized homogeneous regions on the graphite substrate.

ple heat capacity minus a small nonspin contribution determined by a simple extrapolation of the "high"-temperature behavior. The open circles are for a coverage of 0.178, where the transition might be expected to be just completed. The dashed curve shows the results for a somewhat higher coverage, 0.184. The rounded peak near 50 mK, which is emphasized by the log scales, is presumably the remnant of the second-layer fluid, Fig. 6. The amplitude of this peak indicates that ~4% of the second layer remains as a fluid. At 0.181 the fluid contribution has decreased to 2% and at 0.184, as Fig. 15 shows, has almost disappeared. The effect might also be attributable to the inhomogeneity of the surface and to the weakness of the corrugation in the potential implied by the 1-K transition temperature.

The much sharper peak at 2.5 mK, Fig. 15, is due to the nuclear spins in the second layer. The contribution from the spins in the first compressed layer is negligibly small as can be inferred directly from Fig. 6, which shows a very small heat capacity near 2 mK with no measurable exchange tail. Of course, the assumption is that there is no increase in the coupling between layers after the second-layer structural transition takes place.

Following are some observations about the spin peak, many of which argue against the second-layer registered solid being a spin-$\frac{1}{2}$ Heisenberg system on a simple triangular lattice: (1) the peak is sharp as a function of temperature and suggestive of a finite-temperature phase transition; (2) for $T < T_{peak}$, the heat capacity is proportional to T, although the data exist only over a very limited temperature range; (3) for $T \gtrsim T_{peak}$ the temperature dependence of the heat capacity is weaker than $1/T$; (4) T_{peak} is very insensitive to areal density; and (5) the peak is probably associated with antiferromagnetic behavior. This last item is inferred from the data of Franco *et al.*[12] which show that the low-temperature magnetization at this coverage lies below the paramagnetic value. This is contrary to what one would have expected, since for a triangular lattice, three-spin exchange should be the dominant process,[31] and this leads to an effective ferromagnetic interaction. The sharp heat-capacity peak is also surprising, since adsorbed solid ^{3}He is usually considered to constitute a 2D Heisenberg system that cannot order at nonzero temperature.[32] It should be noted, however, that the dipolar interactions, which have a strength of the order of 0.1 μK, may be playing an important role even at mK temperatures, as has been discussed recently by Friedman *et al.*[33] These authors find that the dipolar terms that break the Heisenberg symmetry will cause a 2D system with ferromagnetic exchange to order at a finite temperature determined primarily by the exchange energy J. A similar result may apply for antiferromagnetic exchange.

Figure 16 shows the spin entropy at 0.184 computed by integrating c_{spin}/T, assuming that $c_{spin} \alpha T$ for $T \leq T_{peak}$. Since the heat capacity must tend towards zero at least as the first power of T, one might expect this calculation to yield an upper limit for the entropy. Instead, however, the high-temperature entropy is a factor of 2 smaller than the anticipated $k_B \ln 2$ per second-layer particle. This suggests two possibilities: either the spin system retains significant order at 25 mK, or our assumption of a linear heat capacity below T_{peak} is incorrect. The first of these can be ruled out by the magnetization measurements,[12] which indicate that at the corresponding coverage, the free spin value is reached for all of the spins already at 10 mK. The conclusion, therefore, must be that the heat capacity has a second anomaly below 2 mK, corresponding to the ordering of the remaining half of the nuclear-spin degrees of freedom.

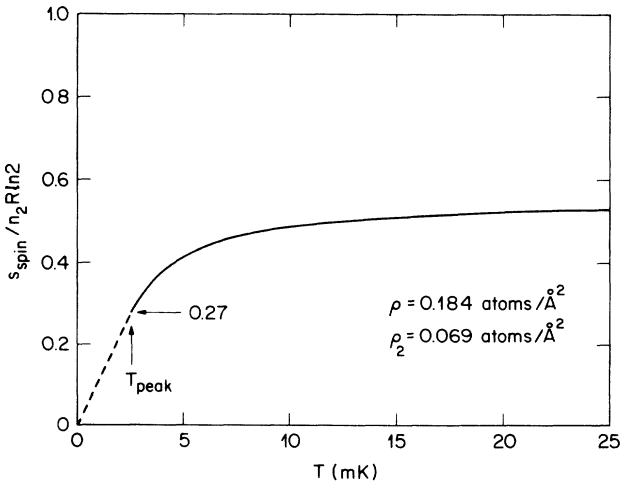

FIG. 16. Nuclear-spin entropy for the second-layer registered phase calculated assuming that the spin heat capacity is proportional to temperature below 2.5 mK.

One possible explanation is that spin polarons form around a finite concentration of zero-point vacancies.[34] This immediately divides the spins into two categories: Those very near a vacancy and those that are more distant. The distant spins would be governed by a small exchange energy and so would order at a very low temperature. The spins forming the polaron itself should behave very differently. A calculation by Heritier and Lederer[35] shows that such two-dimensional polarons can have either ferromagnetic or antiferromagnetic character depending on the lattice structure, and also shows that the heat capacity would be proportional to $T^{-1/2}$. Figure 17 shows the local, effective power-law exponent describing c_{spin} at 0.184 atoms/Å plotted as a function of the temperature. As the temperature window is moved toward T_{peak} from higher temperatures, the exponent does tend toward the predicted value of $-\frac{1}{2}$, providing some support for this theory. What remains difficult to explain is the lack of any significant density dependence in the experimental results. Certainly the number of vacancies should vary rapidly with coverage. It is also difficult to understand why the computed entropy is so close to half the expected value.

A very different explanation of the experimental results has recently been suggested by Elser,[30] which attributes the double-peaked heat capacity to an intrinsic property of the perfect registered structure. Elser proposes that the atoms are arranged as shown in Fig. 18 and indeed numerical calculations[36] have shown that this structure is stable at low temperatures. The larger, lightly shaded atoms are the first-layer atoms that sit on a triangular lattice incommensurate with the graphite substrate. The darker atoms are the second-layer atoms, which form a triangular lattice commensurate with the first layer and with a density relative to the first layer of $\frac{4}{7}$, in agreement with experiment. There are four atoms in the second-layer unit cell. Three of these (A atoms) lie centered above four first-layer atoms at points of low substrate potential, while the fourth (B atom) sits directly above a first-layer atom and therefore at a potential maximum. A consequence of the B atoms not being as well localized as the A atoms is that there are two different two-particle (antiferromagnetic) exchange rates. Two A atoms exchange readily because the B atom hindering the exchange has a high probability of being out of the way. On the other hand, both near neighbors for an AB pair are A atoms, and these are well localized. One should expect, therefore, that $J_2(A,B) < J_2(A,A)$. If detailed calculations indicate, in fact, a very large difference in these exchange energies, then it may be that the B spins are disordered at a temperature well below 2 mK, and this would mean that $\frac{1}{4}n_2R\ln 2$ should be added to the calculated entropy. This is only half of what is needed, but there may be other contributions to the entropy from the near degeneracy in the ground-state spin configurations of the A atoms that could account for the remaining discrepancy. We note also that a large $J_2(A,A)$ would not only explain the large spin heat capacity measured at low temperatures but would also imply antiferromagnetic ordering in agreement with the magnetization results.

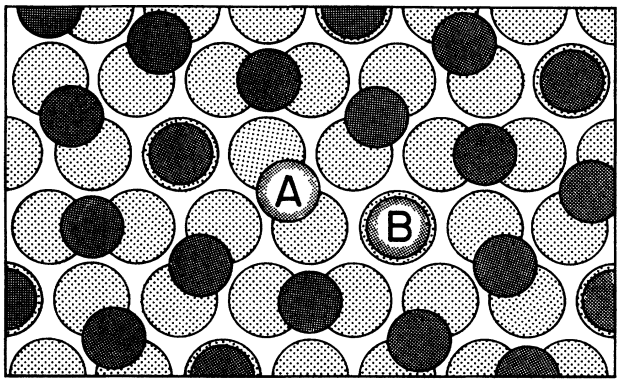

FIG. 18. Structure of the second-layer registered solid proposed by Elser, Ref. 30. One-fourth of the atoms are located directly above first-layer atoms and therefore at substrate potential maxima.

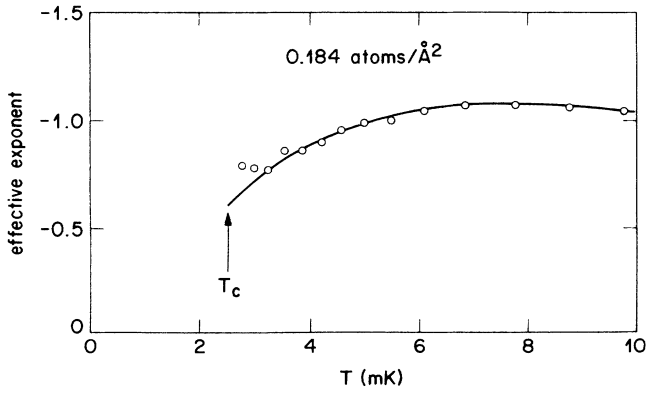

FIG. 17. Effective power-law exponent describing the spin heat capacity of the second-layer registered phase determined using data within a narrow temperature window.

E. Second-layer phase diagram

It is quite clear that the anomaly that occurs in the heat capacity at 2.5 mK prior to third-layer promotion must be associated with the nuclear spins in the second layer. It is less obvious, however, what role the second-layer spins play at higher coverages where the heat-capacity peak evolves into a much more dramatic anomaly. Certainly an indicator of involvement would be correlations between various structural phase changes, which may occur in the second layer, and the several special features in the 2.5 mK isotherm evident from Fig. 7. In this section we infer a second-layer phase diagram based on existing higher-temperature heat-capacity data[4] and on the new low-temperature results presented in this paper.

As the total coverage is increased and atoms are promoted into the third layer, the second-layer density also continues to increase. Consequently, one might expect

the second-layer registered phase to eventually give way to other phases. In fact, this must be the case, since neutron scattering experiments[20] have shown that at a coverage of 0.297 atoms/Å^2 the second layer exists as an incommensurate solid.

Heat-capacity measurements on high-coverage samples should therefore show second-layer melting peaks which, because of the low second-layer density, should occur for temperatures in the vicinity of 1 K. Indeed, heat-capacity peaks have been observed[4] at the appropriate coverages and temperatures, but these have been interpreted as signaling evaporation of three-dimensional clusters. Our belief, however, is that these are actually the sought after peaks and consequently we refer to the temperature of these features as $T_{m,2}$.

Figure 19 shows $T_{m,2}$ plotted versus total coverage. In Van Sciver's original plot of these data, he included one additional point at a coverage of 0.186 and at a temperature of 50 mK. The rise in the heat capacity which he observed at his lowest achievable temperature is, however, due to the nuclear-spin contribution and is thus unrelated to the other points shown in his figure. The saturation of $T_{m,2}$ near $\rho=0.25$ indicates that at this relatively high total coverage the second layer finally approaches its maximum density. The kink near $\rho=0.21$ corresponds to the crossing of a phase boundary. Below this coverage the second layer does not exist at low temperature as a single-phase incommensurate solid. This will be discussed again in the following.

Before proceeding to make the analysis more quantitative, we digress to point out that a small adjustment was applied to the coverage scale used by Van Sciver and Vilches, to bring it into better agreement with our own. The discrepancy was revealed by the different coverages assigned to the freezing of the second layer into the registered phase. They find the second layer to be completely solid at 0.186 while our value is 0.178. The 4.5% difference is larger than we might have expected, but probably is still within the experimental uncertainties.

Away from the coverage region where registry is occurring, the first and second layers should behave in a very similar manner. In particular, we expect the density dependence of the melting temperature for the incommensurate solid to be the same for both layers. That is,

$$\frac{dT_{m,2}}{d\rho_2}\approx\frac{dT_{m,1}}{d\rho_1}=185\ \text{K Å}^2\ , \tag{11}$$

where the numerical value is determined by the monolayer data of Hering *et al.*[36] Combining this relation with the data shown in Fig. 19 allows an estimate of

$$\frac{d\rho_2}{d\rho}\approx\frac{\Delta T_{m,2}/185}{\Delta\rho}\ . \tag{12}$$

Calculated values of this derivative are plotted in Fig. 20(a) for $\rho>0.22$. The solid curve passing through these

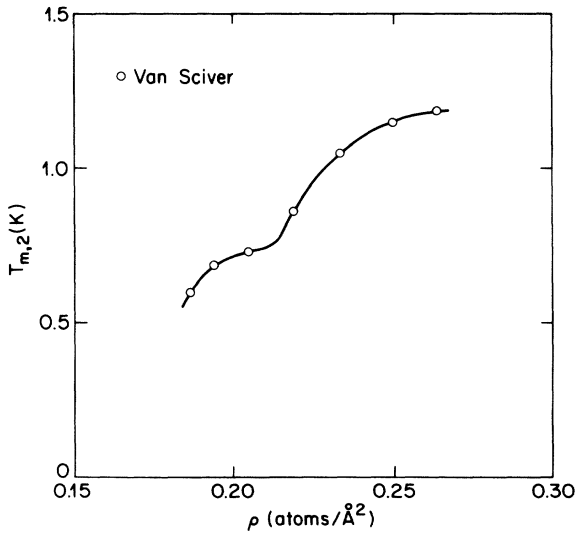

FIG. 19. Temperature of the heat-capacity peaks measured by Van Sciver, Ref. 4, for multilayer ^{3}He films. These peaks were originally ascribed to evaporation of 3D clusters. Our contention is that the data above the kink are due to the melting of the incommensurate second-layer solid. The coverage scale has been adjusted by 4%; see the text.

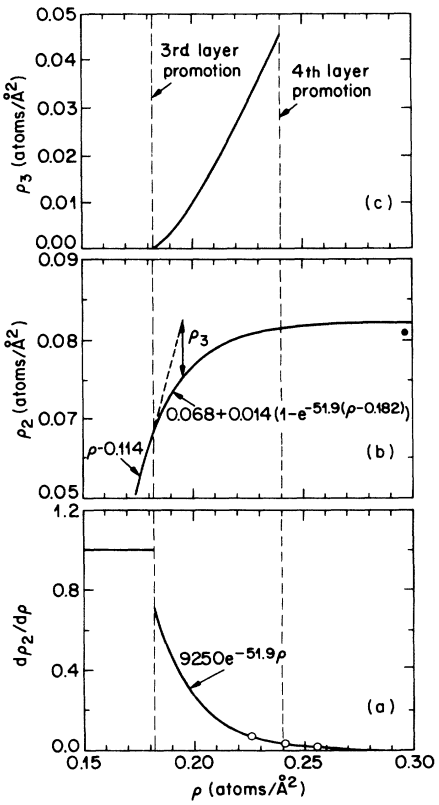

FIG. 20. Second-and third-layer densities as a function of total coverage. The open circles in (a) are derived from the heat-capacity data of Van Sciver, Ref. 4. The solid circle in (b) is a neutron scattering result from Lauter *et al.*, Ref. 20. The analysis leading to the solid curves is described in the text.

three data points is a least-squares fit using the empirical relation

$$\frac{d\rho_2}{d\rho} = ae^{-b\rho} . \tag{13}$$

with best-fit parameters

$$a = 9250 ,$$

$$b = 51.9 \text{ Å}^2 .$$

A check to determine if this function gives a reasonable estimate of this derivative for $\rho \lesssim 0.22$ can be made by simply integrating to obtain ρ_2 as a function of ρ. As Fig. 20(b) shows, the calculated value of ρ_2 saturates at 0.082 which agrees quite well with the result from neutron scattering experiments[20] shown by the solid circle. Note that the calculated ρ_2 is, of course, sensitive to the density used for the compressed first layer. Figure 2(c) shows $\rho_3 \equiv \rho - \rho_1 - \rho_2$ with $\rho_1 = 0.114$.

Some miscellaneous observations based on Fig. 20 follow: (1) Just above third-layer promotion, 70% of the atoms are still going into the second layer. (2) The maximum second-layer density is 75% of the compressed first-layer density. (3) At fourth-layer promotion, the second layer has nearly reached its fully compressed density. (4) Promoted atoms can compress the first layer by only a few percent but can compress the second layer by 20%. (5) Second-layer promotion occurs when $\rho_1 = 0.109$; third-layer promotion occurs when $\rho_2 = 0.070$; and fourth-layer promotion occurs when $\rho_3 = 0.045$.

Figure 21 compares the first-layer phase diagram and the second-layer diagram based on values of ρ_2 derived from the total density using Fig. 20(b). All of the data points shown correspond to the location of heat-capacity peaks[3,4,37,38] that bound very similar regions for both layers. This is the primary motivation for assuming a one-to-one correspondence between the two-phase diagrams and dividing the bounded areas into equivalent regions. *F*, *R*, and *S* stand for fluid, registered phase, and incommensurate solid respectively, while the short horizontal lines near $T = 0$ give phase boundaries determined by these heat-capacity results for the second layer (see Sec. III D and III F 2) and by our interpretation of the data of Hickernell *et al.*[39] for the first layer.

We note that usually the monolayer phase diagram is

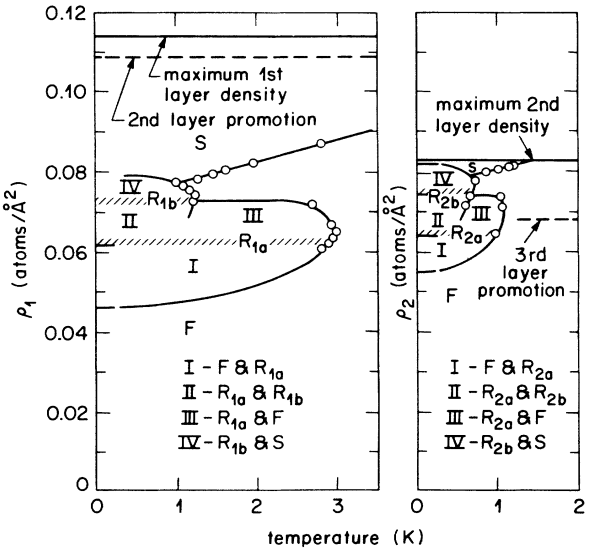

FIG. 21. Comparison of the first- and second-layer phase diagrams proposed for ^{3}He on graphite. All of the data points correspond to heat-capacity peaks from Refs. 3, 4, 37, and 38. The determination of the second-layer density is described in the text. *F*, *R*, and *S* refer to fluid, registered phase, and incommensurate solid, respectively.

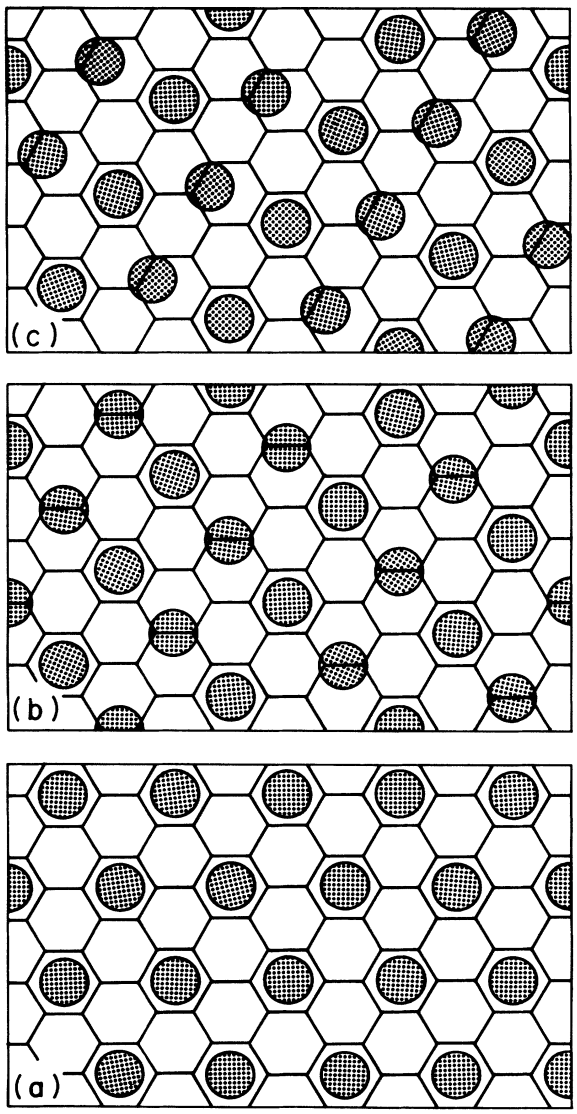

FIG. 22. Registered structure for monolayers of ^{3}He on the basal plane of graphite. (a) shows the $\sqrt{3}$ phase corresponding to R_{1a} in Fig. 21. (b) and (c) show possible structures for the R_{1b} phase with $\frac{2}{5}$ of the graphite hexagons being occupied by ^{3}He atoms.

presented with an indication of only a single registered phase which is associated with the large density region centered at 0.064 atoms/Å^2. The implication is that the registered phase exists at the lower coverages with a large concentration of vacancies and at the higher coverages with a large concentration of interstitials.[34] This is not consistent with our second-layer experimental data. Certainly there may be a range of densities over which the registered phase exists with vacancies or with interstitials, but this range must be rather small and has been allowed for by the shading in both the first- and second-layer diagrams. At 0.064 the registered phase R_{1a}, corresponds to a triangular lattice with one out of three graphite adsorption sites occupied by a helium atom, Fig. 22(a). Based on a comparison with the second-layer diagram it is proposed that another registered phase, R_{1b}, exists near 0.076. This is supported by the sharp heat-capacity peaks[29] observed in this coverage regime and also by the weak density dependence of the peak temperature. Two possible striped structures for this phase, with two atoms for every five adsorption sites, are indicated in Figs. 22(b) and 22(c). For first- and second-layer coverages somewhat higher than those corresponding to R_{1b} and R_{2b}, the systems exist in states intermediate between the commensurate and incommensurate solids. These states[40] may be more complicated than simple two-phase coexistence.

Although qualitatively the two-phase diagrams appear to be extremely similar, note that registry in the first layer is relative to the graphite substrate, while registry in the second layer is relative to the underlying triangular lattice of the first compressed ^{3}He layer. The lower melting temperature of the second-layer registered solid simply reflects the weaker corrugation in the potential experienced by the second-layer atoms.

F. More than two layers; $0.182 < \rho \leq 0.370$ atoms/Å^2

This coverage regime begins with fluid atoms being promoted into the third layer, over a substructure consisting of two solid ^{3}He layers. The first of these layers exists as a fully compressed incommensurate solid and the second as a low-density registered solid. As the total coverage increases above 0.182, the second-layer density also increases and phase changes occur in this layer. Above roughly 20 mK, the heat capacity is dominated by the contributions from the developing third, fourth, and fifth fluid layers. At lower temperatures, the heat-capacity peak associated with the second-layer nuclear spins transforms into a larger anomaly which reaches a maximum amplitude at $\rho=0.24$. It is this anomaly which is the main topic of this section. We begin by discussing the separation of the measured heat capacity into spin and nonspin components.

1. Extraction of the nuclear-spin contribution to the heat capacity

Because the nuclear-spin and the fluid components of the heat capacity dominate in different temperature regions it might appear that the separation of the two contributions could be accomplished with little ambiguity. In practice, however, there are complications, particularly for coverages near 0.24. The main problem arises from the fact that the spin heat capacity does not decay rapidly with increasing temperature and remain significant over the temperature range where the fluid term should be linear in temperature. There is also the complication of a third contribution to the heat capacity. In Sec. III B it was noted that a small temperature-independent contribution to the heat capacity develops abruptly as atoms are promoted into the second layer. At higher coverages this contribution increases as atoms are promoted into the third and subsequent layers. It is assumed that this term retains its temperature independence and we continue to refer to this term using the parameter β.

The most reliable values of β are obtained from the data at the highest coverages, because here the spins provide only a small contribution to the total heat capacity, Fig. 6. These data were fit using the expression

$$c=\frac{\alpha}{T^2}+\beta+\gamma T \tag{14}$$

over the temperature range between 5 and 20 mK. The low-temperature limit was set sufficiently high so that a more accurate function describing the spin term was not required. The high-temperature limit was set sufficiently low so that the term linear in T was adequate to describe the fluid contribution. At $\rho=0.37$ the fit yielded $\beta=0.44$ mJ/K. Fits performed at progressively lower coverages yielded values of β which generally decreased in magnitude but with a rapidly increasing uncertainty.

The expression

$$\beta=1.70\rho-0.190\ , \tag{15}$$

which we use to approximate β for $0.182\leq\rho\leq0.370$, is consistent with the best-fit results obtained for $0.24\leq\rho\leq0.37$ and with $\beta=0.12$ mJ/K found for the two-layer system, Sec. III C. Note that the high-coverage value of β is roughly four times larger than 0.12 indicating an increase in β of about the same magnitude for each layer promotion.

Using Eq. (15) to determine fixed values of β, the data at each coverage were again fit using Eq. (14), now to obtain, primarily, the parameter γ. The fits were performed over three temperature ranges: $10<T<30$, $15<T<30$, and $10<T<20$ mK. For data corresponding to $0.24\leq\rho\leq0.37$, the rms deviation of each of the fits was less than several tenths of a percent, and the three values of γ for each coverage differed by at most 2%. The same type of analysis could not be extended to coverages below 0.24 because here the rms deviations abruptly increased, indicating that Eq. (14) was no longer adequate to describe the data. Of course the failure of Eq. (14) at the lower coverages was anticipated, because at third-layer promotion the spin heat capacity (Sec. III D) clearly varies much slower than $1/T^2$. In fact, just prior to third-layer promotion, the spin heat capacity varies as $T^{-0.872}$ in the temperature range between 3 and 8 mK. An attempt was therefore made to fit the data with $0.184\leq\rho\leq0.24$ using the expression

$$c-\beta=\alpha/T^{0.872}+\gamma T \ . \tag{16}$$

At coverages of 0.184, 0.190, and 0.200 the rms deviations are a few tenths of a percent for data in the temperature range between 20 and 40 mK. The temperature window was set higher than in the previous fits because of the slower falloff of the spin contribution, and because of the smaller fluid heat capacity. At coverages of 0.21, 0.22, and 0.23, the rms deviations were significantly larger than at the lower coverages. For this reason the γ values for these coverages were determined by a simple graphical interpolation of the γ values found for the higher- and lower-coverage regions. In the remainder of this paper the spin contribution to the heat capacity is defined by

$$c_{\text{spin}}=c-\beta-\gamma T \tag{17}$$

with the values of β and γ for each coverage listed in Table II.

The spin heat-capacity results are plotted on log-log scales in Fig. 23, with the lower portion of the figure showing curves for $\rho \leq 0.24$ and the upper portion showing curves with $\rho \geq 0.24$ atoms/Å^2. At the lower coverages the results show a complicated evolution towards a $1/T^2$ behavior as the peak heat capacity at 2.5 mK grows towards it maximum amplitude. This is in contrast to the much simpler behavior observed at the higher coverages where it is only the amplitude and not the overall temperature dependence which is changing.

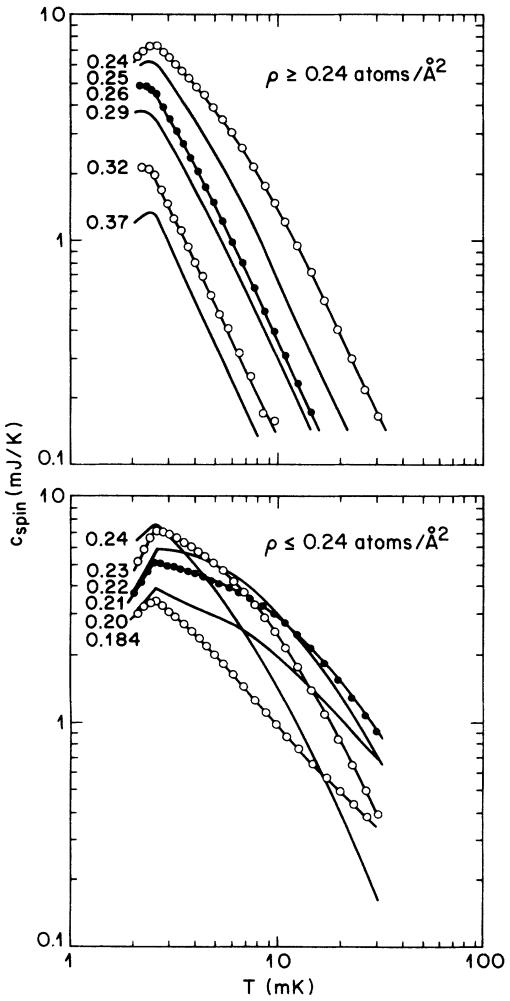

FIG. 23. Nuclear-spin heat capacity due to the atoms in the second layer.

2. *The anomaly peaked at $\rho=0.24$ atoms/Å^2*

In the work of Franco *et al.*,[2] it was proposed that the large magnetization anomaly which they observed at a coverage of 0.24 atoms/Å^2 (Fig. 7) was due to the ^{3}He atoms in the second adsorbed layer and developed as this second layer solidified. They argued that since the low-coverage side of their peak was linear in coverage it was consistent with a two-phase coexistence of fluid and solid. The decrease on the high-coverage side of the peak was associated with the compression of the completed solid layer and the expected drop in the exchange energy with increasing density. In this section we present a very different physical picture based on the new information provided by the heat-capacity results. As was already discussed in Sec. III D, our data indicate that the second layer solidifies into a registered phase prior to third-layer promotion. This immediately implies, contrary to the model of Franco *et al.*, that one should not expect fluid-solid coexistence in the coverage regime near 0.24. We do agree, however, that the large magnetic anomaly should be associated with the second-layer atoms.

If the region $0.21 \leq \rho \leq 0.24$ atoms/Å^2 does not correspond to fluid-solid coexistence can it correspond to some other type of two-phase coexistence in the second layer? Certainly if it did and if the second layer could be treated as an independent system, then the magnetization and also the heat capacity along isotherms should vary linearly with the *second-layer* density. Since ρ_2 is not linearly related to ρ (Sec. III E) we should not expect these thermodynamic quantities to vary linearly with total coverage. Of course there may be complicated intralayer interactions or significant interactions between atoms in different layers, and so the observed coverage dependence may be very different from ideal behavior. In any case, at a coverage corresponding to either the onset or the termination of an intermediate phase region there should be an abrupt change in behavior evident in *all* of the appropriate isotherms. In the magnetization results there is a peak in the 3 mK isotherm at 0.24, but no sharp feature in any of the higher-temperature isotherms at this same coverage. This is also true for the heat-capacity data. The 5-mK isotherm in Fig. 7, which like the 2.5-mK curve, is dominated by the spin contribution to the heat capacity, does not show any special feature at 0.24. Instead there is a rounded peak centered at a lower coverage. From this it is concluded that $\rho=0.24$ does not correspond to a phase boundary; the sharp peaks in the 3-mK magnetization isotherm and in the 2.5-mK heat capacity isotherm must arise for other reasons.

Note that promotion of atoms into the fourth layer also occurs at 0.24 atoms/Å^2, Fig. 7. It is difficult, how-

ever, to place any special significance on this correlation since again there is no obvious correlation with the features in the 5-mK isotherm. Although 0.24 is not a phase boundary one would expect second-layer phase boundaries to be crossed in this general vicinity based on the second-layer phase diagram Fig. 21. The sudden changes in behavior at $\rho=0.18$, at 0.19, and at 0.26 seen in both the 2.5- and 5-mK isotherms, Fig. 7, we believe correspond to these expected boundaries. Since these second-layer effects occur in the spin contribution to the heat capacity we naturally conclude that the spin heat capacity at these higher coverages continues to arise from the second-layer atoms. This is also the conclusion reached by Franco *et al.*[12] based on the value of the Curie constant at "high" temperature. Evidence that the second-layer atoms are mainly responsible for the spin heat capacity can also be obtained from the spin entropy which is discussed in Sec. III F 4.

Since the spin heat capacity is believed to be due to the second-layer atoms, c_{spin} isotherms are plotted most meaningfully as a function of ρ_2. Curves for 3, 5, and 10 mK are shown in Fig. 24. For reference the total density is indicated at the top of the figure. The changes in behavior occurring for all three isotherms at $\rho_2\approx0.064$ and at 0.074 locate the phase boundaries which correspond to the kinks in the low-temperature isotherms shown in Fig. 7 at total coverages of 0.178 and 0.193. The kink at $\rho=0.26$ also seen in Fig. 7, which locates another boundary, corresponds to $\rho_2\approx\rho_2^{\max}$ and is therefore not observable in Fig. 24.

We consider first the region $0.064<\rho_2<0.074$ which is characterized by c_{spin} changing only weakly with ρ_2. This weak dependence is surprising since at $\rho_2=0.064$ the second layer exists as a registered phase. Consequently, as ρ_2 is increased one would expect c_{spin} to change dramatically, as the system moves away from perfect registry. The fact that this does not occur suggests that perhaps the second-layer density might not actually be changing as much as Fig. 20 implies.

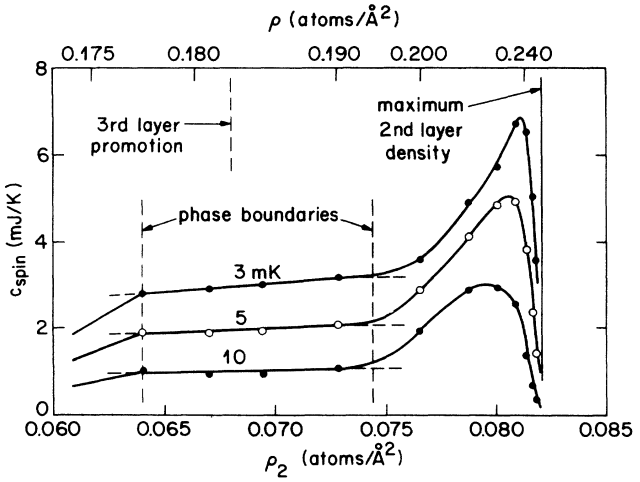

FIG. 24. Second-layer spin heat capacity as a function of second-layer density. For $0.055<\rho_2<0.064$ atoms/Å^2 there is a coexistence between a fluid and a registered range. For $0.064<\rho_2<0.074$ there may be coexistence between two registered phases. The region $0.074<\rho_2<0.082$ corresponds to an intermediate state between the registered and incommensurate solids. For the very narrow region between 0.082 and $\rho_2^{\max}$ the second layer exists as an incommensurate solid.

It is possible that the second-layer registered phase initially resists the loss of complete registration by promoting excess atoms into the third layer. With increasing coverage some of these third-layer atoms would eventually be demoted back into the second layer. This might occur at $\rho=0.193$, where we see the rather sudden change in c_{spin}. Arguing against this type of behavior, however, is the fact that layer promotion does not occur coincident with the completion of the registered phase at $\rho_2=0.064$, but instead at a somewhat higher coverage, namely $\rho_2=0.068$.

Another possibility is also suggested by Fig. 24 since c_{spin} is proportional to ρ_2. Of course this also means that c_{spin} is proportional to N_2. Each second-layer atom therefore makes about the same contribution to the total spin heat capacity, independent of the number of atoms in the second layer. This may mean that the actual second-layer registered phase density (as opposed to the average second-layer density plotted in Fig. 24) is not changing, as would be the case if the atoms are being added to "condensed" regions. These condensed regions might be centered in each of the homogeneous regions provided by the graphite substrate. If this interpretation is correct then complete registry does not occur at $\rho_2\approx0.064$ but instead at 0.074. This latter density corresponds to a fractional coverage $\rho_2/\rho_1=0.074/0.114\approx\frac{2}{3}$ which implies a different class of possible registered structures. A second layer, which is partially fluid in this coverage regime, is qualitatively consistent with the heat-capacity data, Fig. 15, which show an anomaly near 50 mK. Quantitatively, however, this model implies that roughly half of the second layer should be fluid at $\rho_2=0.064$ ($\rho=0.178$), and this is difficult to reconcile with the experimental results.

It appears most probable that the linear coverage dependence of the heat capacity for $0.065<\rho_2<0.074$ is indicating a two-phase coexistence between two different registered phases; see Fig. 21. The lower-density phase, R_{2a}, has $\rho_2/\rho_1=\frac{4}{7}$ and the higher density phase, R_{2b}, has $\rho_2/\rho_1=\frac{2}{3}$. The difficulty now is to explain the very similar spin heat-capacity signatures of the two registered phases.

Note that according to any of these three models, there is complete registration of the second layer at $\rho=0.193$. In the following, we tacitly assume the second or third of these models in order to continue to make reference to Fig. 24, with ρ_2 referring to the average second-layer density. We note that neutron scattering measurements which give ρ_2 as a function of ρ would be helpful in understanding this coverage regime.

Although there is a change in behavior at $\rho_2=0.074$ for each of the isotherms there is no discontinuity. This again suggests some type of two-phase coexistence at the higher coverages even though the isotherms in this region

are not described by straight lines. The more complicated coverage dependence could possibly be indicating a registered solid with high-density domain walls or perhaps a more usual two-phase coexistence between the registered and incommensurate solids, but with significant interlayer spin interactions involving one or both of the second-layer phases. Still another possibility is that a portion of the registered phase melts into a high-density fluid. This fluid may physically separate regions of registered phase and incommensurate solid. But whatever the nature of this intermediate phase regime, it is here that the ferromagnetic anomaly occurs. It is also likely that third-layer atoms are also playing an important role, such as mediating the indirect exchange of second-layer atoms in a manner similar to that proposed by Jichu and Kuroda.[41]

Assuming ordinary two-phase coexistence, are either of the two phases (S or R) giving the dominant contribution to c_{spin} in the coexistence region? If the R phase is the more dominant phase, then the increase in c_{spin} for $\rho_2 < \rho_2^{\text{peak}}$ might be mainly due to the increasing number of third-layer atoms, while the decrease for $\rho_2 > \rho_2^{\text{peak}}$ might be due to the diminishing fraction of R phase. On the other hand, we know that out-of-plane exchange must be significant for the S phase since at high second-layer densities, where we expect the second layer to exist as pure S phase, the exchange energy is much larger than for monolayer films at comparable first layer densities. This is discussed in the following subsection. If the S phase is giving the dominant contribution to the heat capacity then the low-coverage side of the peak could be explained as being due to both the increasing fraction of S phase and the increasing density of third-layer atoms. The turnaround in c_{spin} at ρ_2^{peak} might be indicating a breakdown of the indirect exchange interaction related to the high density of the third layer and to the large effective mass of the third-layer quasiparticles.[42] Evidence suggesting that it is the S phase which is mainly responsible for the peak at $\rho = 0.24$, is the fact that the peak corresponds to ferromagnetic behavior and also the fact that c_{spin} is nearly proportional to $1/T^2$. This is the temperature dependence which is clearly observed at the highest coverages where the second layer with ferromagnetic properties should be completely incommensurate solid.

The speculation that a dense second-layer fluid may also exist in the intermediate regime is based on Fig. 25 which shows the lower coverage spin heat-capacity results plotted relative to the data at 0.184 atoms/Å^2. It is intriguing that the "excess" heat capacity does not show an anomaly at 2.5 mK corresponding to the growth of the spin heat-capacity peak as a function of coverage, at least for $\rho \leq 0.23$. Instead it appears that the spin peak increases in amplitude mainly as a consequence of a growing rounded maximum near 5 mK that gradually shifts towards 2.5 mK and sharpens as the coverage approaches 0.24. The coverage and temperature dependence of this new contribution is reminiscent of the data for the 2D fluid (Sec. III D), except that here the maxima are shifted to much lower temperatures and culminate, at 0.24 atoms/Å^2, in a sharp solidlike peak at 2.5 mK. It is

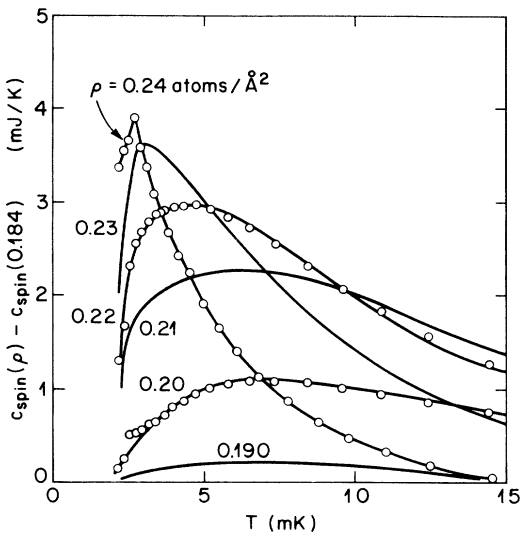

FIG. 25. Increase in the spin heat capacity relative to the results of 0.184 atoms/Å^2. The "excess" heat capacity is reminiscent of the results for a 2D fluid except that the rounded maxima are shifted to much lower temperatures.

therefore possible that a fluid is directly responsible for the ferromagnetism in the second layer. This is consistent with the conclusion of Ref. 25, for the ^{3}He-on-silver system.

3. 2D Heisenberg system

In the recent work of Godfrin, Ruel, and Osheroff,[43] magnetization measurements were made at a coverage near 0.24 atoms/Å^2 and for temperatures extending down to 0.7 mK. These authors found that the second-layer magnetization is well described by a nearest-neighbor Heisenberg Hamiltonian with a ferromagnetic exchange energy of 2.1 mK. Note that this simple form of the Heisenberg Hamiltonian is expected if three-particle ring exchange is giving the dominant spin interaction. Our findings, however, are quite different as can be immediately inferred from the simple fact that at about the same coverage the heat capacity, as a function of temperature, continues to show a sharp *peak* at 2.5 mK. The heat capacity of the ideal two-dimensional Heisenberg system should show only a rounded maximum[32] since this system cannot order at nonzero temperature.

To emphasize the deviations from the expected $1/T^2$ behavior at high temperatures, Fig. 26 gives $c_{\text{spin}}\ T^2$ plotted versus temperature at total coverages of 0.24, 0.25, and 0.26 atoms/Å^2. The dashed and solid curves show the 8 and 10 term series results[44] for the Heisenberg nearest-neighbor ferromagnetic with the exchange energies adjusted to give agreement with the data near 20 mK. Note that J/k_B is 1.7 mK at 0.24 which is close to the value found by Godfrin *et al.*[12] The theoretical curves deviate from the data by roughly 20% at $T \approx 4J/k_B$ for the two lower coverages even though we would expect, based on the comparison of the 8 and 10 term series results, that the theoretical curves should be

valid down to lower temperatures. At a coverage of 0.26 the situation is quite different, with the calculated curves agreeing with the data to within the precision of the measurements. The abrupt change in behavior lends support to our claim that at $\rho=0.26$ there is a transition in the second layer, from "two-phase" coexistence to single-phase incommensurate solid. If the incommensurate phase is giving the dominant contribution to c_{spin} at 0.24 then the number of contributing atoms is roughly 10% less than the total number of second-layer atoms, and it was this latter quantity which was used in preparing Fig. 24. Making the 10% adjustment, however, improves the quality of the fit only slightly. It should also be noted that altering the nonspin contributions which were subtracted from the total heat capacity to obtain c_{spin}, affects mainly the higher-temperature data and causes deviations away from $1/T^2$ behavior near 20 mK.

It is not clear why the heat-capacity data at $\rho=0.24$ depart from the ideal Heisenberg behavior while the magnetization results do not. A possible explanation may be that the magnetization results were obtained in nonzero fields. It may also be that the heat capacity can provide a more sensitive text, since, contrary to the magnetization, it does not tend towards a saturation value at low temperatures.

Above 0.26, the second layer exists as a pure incommensurate solid with the second-layer density asymptotically close to its maximum value. Nonetheless, we would expect a measurable decrease in the exchange energy at higher coverages because of its expected strong dependence on the density. Note that for bulk bcc solid ^{3}He, $J\alpha\rho^{-20}$. Consistent with this expectation we find that above 0.26, c_{spin} monotonically decreases with increasing ρ, Fig. 7. This should be accompanied by a monotonic decrease in the temperature corresponding to the maximum in the heat capacity, but this is not what is observed at the highest coverages. Our explanation is that the peaks in the data for coverages greater than roughly 0.30 are spurious. They are most likely due to an improper subtraction of the nonspin terms, which become relatively very large for large ρ. Assuming that the β term (Sec. III F) is strictly temperature-independent causes an overcorrection at the lowest temperatures, which can become significant at the highest coverages.

An estimate of the exchange energy can be made which bypasses potential problems with the lowest-temperature, highest-coverage data by considering only the coefficient of the $1/T^2$ term of c_{spin} and using the high-temperature expression

$$c_{\text{spin}}=\tfrac{9}{4}n_2R(J/k_BT)^2 . \tag{18}$$

This relation is appropriate for nearest-neighbor exchange on a triangular lattice. The $1/T^2$ coefficients plotted in Fig. 27 as a function of total coverage were determined using plots similar to Fig. 26. The corresponding exchange energies are given by the scale at the right side of the figure. At 0.26 atoms/Å^2, the exchange energy of the two-dimensional solid is 0.85 mK. This falls to 0.41 mK at $\rho=0.37$ and to roughly 0.2 mK in the high-coverage limit. This last energy is derived from magnetization results.[8] Magnetization measurements[12] also yield exchange energies of 0.55 mK at 0.27 atoms/Å^2 and of 0.33 mK at 0.28 atoms/Å^2, if the Weiss temperatures actually reported are converted to J values using the simple relation $J/k_B=\theta_W/3$. These energies are somewhat smaller than the values extracted from the

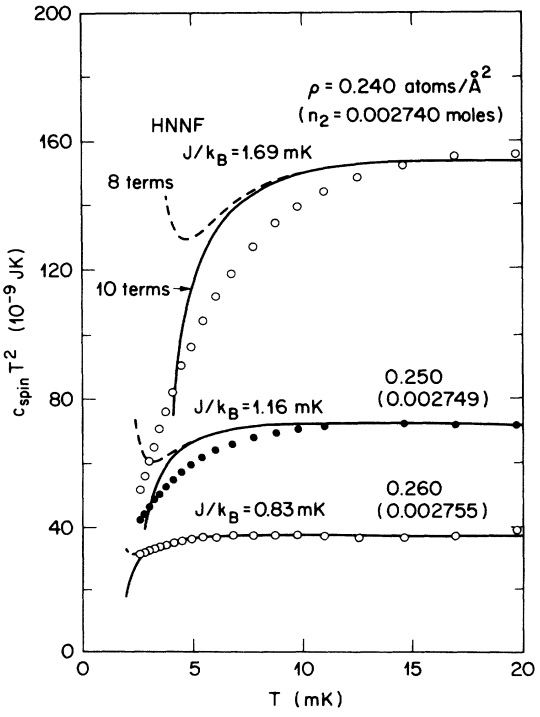

FIG. 26. Comparison of the spin heat capacities measured for coverages near the ferromagnetic anomlay with those calculated using the 8- and 10-term series expressions for the nearest-neighbor Heisenberg Hamiltonian.

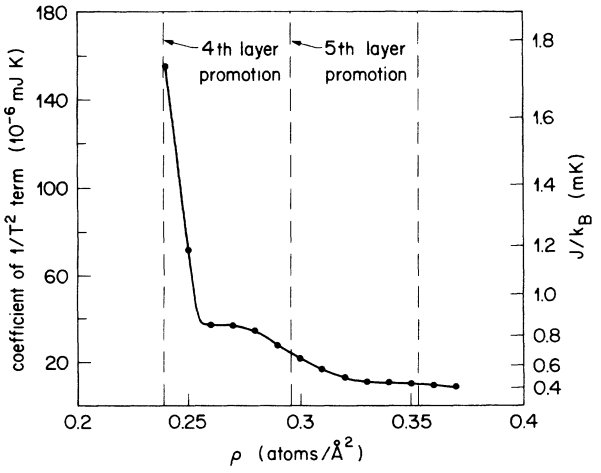

FIG. 27. Exchange energy for the second-layer solid extracted from the spin contribution to the heat capacity.

heat-capacity data and also show a stronger density dependence. We note that in the more recent work of Godfrin *et al.*[43] an improved analysis of the magnetization data obtained near $\rho=0.24$ increased J by nearly a factor of 2. It may be that a similar reanalysis of the higher-coverage data will also shift these values upwards toward better agreement with the heat-capacity energies.

A comparison of the exchange energies for the first and second incommensurate solid layers at the same layer densities shows that they differ by nearly an order of magnitude. The implication is that strictly in-plane exchange cannot be responsible for the dominant spin interaction in both of these layers. The density dependence of J for the second layer is also difficult to explain without invoking out-of-plane interactions. Between $\rho=0.28$ and $\rho=0.31$, Fig. 27 shows that J changes by 45%. Even if an extremely strong density dependence is assumed, such as $J\alpha\rho_2^{-20}$, the change in J due to second-layer density changes alone should be at most a few percent. More direct indicators for interactions between the atoms in the second layer and those in the higher fluid layers are the cusps in the 200-mK isotherm (Fig. 7) at $\rho=0.26$ and 0.32 which correlate with the changes in the coverage dependence of the second-layer spin heat capacity (see Figs. 7 and 27).

4. *Spin entropy at $\rho=0.24$ atoms/Å^2*

Figure 28 shows the second-layer spin entropy at $\rho=0.24$ atoms/Å^2 computed using the smoothed c_{spin} results. At high temperatures the limiting entropy falls 10–15 % below n_2R ln2. This is analogous to the much larger entropy discrepancy discussed in Sec. III D in regard to the registered phase at $\rho=0.184$ and again indicates that the assumption of a linear c_{spin} for $T<T_{\text{peak}}$ is incorrect. Ordering of some of the spin degrees of freedom must be occurring below 2 mK which is not accounted for by a linear heat capacity at low temperatures. But this is exactly as we would expect since our claim is that $\rho=0.24$ corresponds to a "two-phase" region and we know that roughly half of the spin entropy of the registered phase is removed at temperatures well below T_{peak}. The measurements of Godfrin *et al.*[43] at $\rho=0.233$ also appear consistent with two-phase coexistence since their magnetization extrapolated to zero temperature falls roughly 20% short of the saturation value computed for all second-layer atoms.

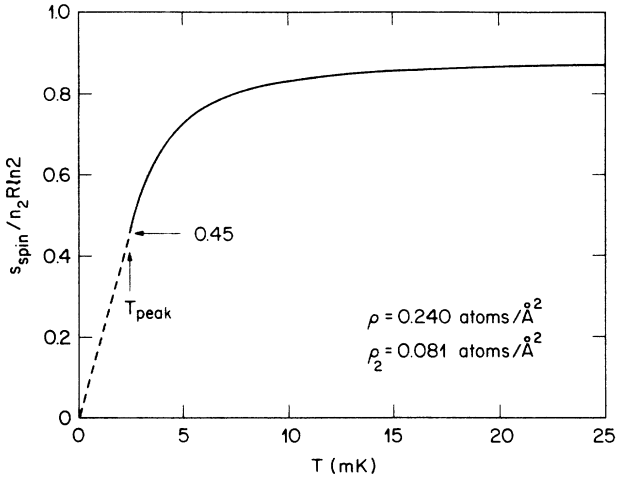

FIG. 28. Nuclear-spin entropy for the second layer at a coverage corresponding to the ferromagnetic anomaly. The entropy was calculated assuming that the spin heat capacity is proportional to temperature below 2.5 mK.

As a final comment we note that because the spin entropy and magnetization tend toward values that are close to, but somewhat smaller than, the limits expected for the second layer, there is no evidence that third- or fourth-layer fluid atoms are directly contributing to the ferromagnetic anomaly.

ACKNOWLEDGMENTS

We are grateful to M. H. W. Chan, V. Elser, H. Godfrin, and O. E. Vilches for many valuable discussions. We are also indebted to O. E. Vilches for his measurement of the krypton isotherm on our Grafoil sample and to Paul A. Busch for his expert technical assistance.

[1]M. Bretz, J. G. Dash, D. C. Hickernell, E. O. McLean, and O. E. Vilches, Phys. Rev. A **8**, 1589 (1973).

[2]J. G. Dash, *Films on Solid Surfaces* (Academic, New York, 1975).

[3]S. W. Van Sciver and O. E. Vilches, Phys. Rev. B **18**, 285 (1978).

[4]S. W. Van Sciver, Phys. Rev. B **18**, 277 (1978).

[5]D. F. Brewer and J. S. Rolt, Phys. Rev. Lett. **29**, 1485 (1972).

[6]A. I. Ahonen, J. Kokko, O. V. Lounasmaa, M. A. Paalanen, R. C. Richardson, W. Schoepe, and Y. Takano, in *Quantum Fluids and Solids*, edited by S. B. Trickey, E. D. Adams, and J. W. Duffy (Plenum, New York, 1977), p. 171.

[7]A. I. Ahonen, T. A. Alvesalo, T. Haavasoja, and M. C. Veuro, Phys. Rev. Lett. **41**, 494 (1978); Proceedings of the 15th International Conference on Low Temperature Physics, Grenoble, 1978 [J. Phys. (Paris) C **6**, 285 (1978)].

[8]H. M. Bozler, T. Bartolas, K. Luey, and A. L. Thomson, Phys. Rev. Lett. **41**, 490 (1978); Proceedings of the 15th International Conference on Low Temperature Physics, Grenoble, 1978 [J. Phys. (Paris) C **6**, 283 (1978)].

[9]H. J. P. Godfrin, G. Frossati, D. Thoulouze, M. Chapellier, and W. G. Clark, Proceedings of the 15th International Conference on Low Temperature Physics, Grenoble, 1978 [J. Phys. (Paris) C **6**, 287 (1978)].

[10]T. Haavasoja, Ph.D. thesis, Helsinki University of Technology, 1980 (unpublished); T. A. Alvesalo, T. Haavasoja, and M. T. Manninen, J. Low Temp. Phys. **45**, 373 (1981); T. A. Alvesalo, T. Haavasoja, and M. T. Manninen, and A. T. Soinne, Phys. Rev. Lett. **44**, 1076 (1980).

[11]D. S. Greywall, Phys. Rev. B **33**, 7520 (1986).

[12]H. Franco, R. E. Rapp, and H. Godfrin, Phys. Rev. Lett. **57**, 1161 (1986).

[13]D. S. Greywall and P. A. Busch, Phys. Rev. Lett. **62**, 1868 (1989).

[14]Grafoil is an exfoliated graphite manufactured by Union Carbide.
[15]D. S. Greywall and P. A. Busch, Rev. Sci. Instrum. **60**, 471 (1989).
[16]H. Godfrin (private communication).
[17]D. S. Greywall and P. A. Busch, J. Low Temp. Phys. **46**, 451 (1982).
[18]M. H. W. Chan, A. D. Migone, K. D. Miner, and Z. R. Li, Phys. Rev. B **30**, 2681 (1984).
[19]H. J. Lauter, H. Wichert, and R. Feile, in *Proceedings of the International Conference on Ordering in Two Dimensions, Lake Geneva, Wisconsin, 1980,* edited by S. K. Sinha (North-Holland, New York, 1980); K. Carneiro, L. Passell, W. Thomlinson, and H. Taub, Phys. Rev. B **24**, 1170 (1981).
[20]H. J. Lauter, H. P. Schildberg, H. Godfrin, H. Wiechert, and R. Haensel, Can. J. Phys. **65**, 1435 (1987).
[21]O. E. Vilches (private communication).
[22]S. V. Hering and O. E. Vilches, in *Monolayer and Submonolayer Helium Films,* edited by J. G. Daunt and E. Lerner (Plenum, New York, 1973), p. 1.
[23]B. Cowan, L. Abou El-Nasr, M. Fardis, and A. Hussain, Phys. Rev. Lett. **58**, 2308 (1987).
[24]H. Godfrin (unpublished).
[25]D. S. Greywall and P. A. Busch, Phys. Rev. Lett. **60**, 1860 (1988).
[26]D. S. Greywall, Phys. Rev. B **27**, 2747 (1983).
[27]E. O. McLean, Ph.D. thesis, University of Washington, 1972 (unpublished).
[28]C. Tiby, H. Wichert, H. J. Lauter, and H. Godfrin, Physica (Amsterdam) **107B&C**, 209 (1981).
[29]S. V. Hering, S. W. Van Sciver, and O. E. Vilches, J. Low Temp. Phys. **25**, 793 (1976).
[30]V. Elser, Phys. Rev. Lett. **62**, 2405 (1989).
[31]M. Roger, Phys. Rev. B **30**, 6432 (1984).
[32]L. J. deJongh and A. R. Miedema, Adv. Phys. **23**, 1 (1974).
[33]L. J. Friedman, A. L. Thomson, C. M. Gould, and H. M. Bozler, Phys. Rev. Lett. **62**, 1635 (1989).
[34]R. A. Guyer, Phys. Rev. Lett. **39**, 1091 (1977).
[35]M. Heritier and P. Lederer, Phys. Rev. Lett. **42**, 1068 (1979).
[36]F. F. Abraham, J. Q. Broughton, P. W. Leung, and V. Elser (unpublished).
[37]S. V. Hering, S. W. Van Sciver, and O. E. Vilches, J. Low Temp. Phys. **25**, 793 (1976).
[38]M. Bretz, J. G. Dash, D. C. Hickernell, E. O. McLean, and O. E. Vilches, Phys. Rev. A **8**, 1589 (1973), and references therein; Phys. Rev. A **9**, 2814(E) (1974).
[39]D. C. Hickernell, E. O. McLean, and O. E. Vilches, Phys. Rev. Lett. **28**, 789 (1972).
[40]S. N. Coppersmith, D. S. Fisher, B. I. Halperin, P. A. Lee, and W. F. Brinkman, Phys. Rev. B **25**, 349 (1982).
[41]H. Jichu and Y. Kuroda, Prog. Theor. Phys. **67**, 715 (1982).
[42]S. Tasaki, Prog. Theor. Phys. **79**, 1311 (1988).
[43]H. Godfrin, R. R. Ruel, and D. D. Osheroff, Phys. Rev. Lett. **60**, 305 (1988).
[44]G. A. Baker, H. E. Gilbert, J. E. Rushbrooke, and G. S. Rushbrooke, Phys. Lett. **25A**, 207 (1967).

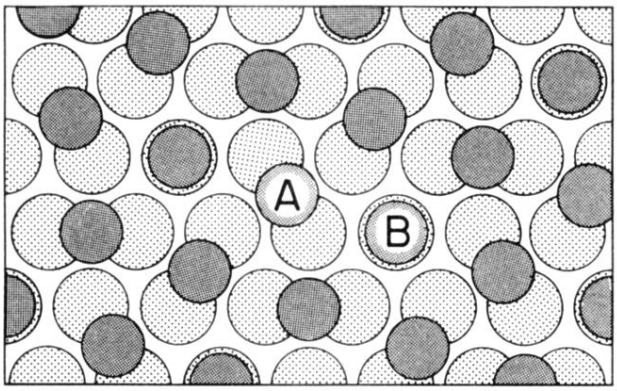

FIG. 18. Structure of the second-layer registered solid proposed by Elser, Ref. 30. One-fourth of the atoms are located directly above first-layer atoms and therefore at substrate potential maxima.